Recent Advances in Orientation of Conjugated Polymers for Organic Field-Effect Transistors

Manish Pandey [‡*a], Nikita Kumari[a], Shuichi Nagamatsu[b], Shyam. S. Pandey[*a]

[a]Division of Green Electronics, Graduate School of Life Science and Systems Engineering, Kyushu Institute of Technology, 2-4 Hibikino, Wakamatsu, Kitakyushu 808-0196, Japan

[b]Department of Computer Science and Electronics, Kyushu Institute of Technology, Iizuka, 820-2502 Japan

[‡]Present Address: Laboratory for Organic Electronics, Division of Materials Science, Graduate School of Life Science and Systems Engineering, Kyushu Institute of Technology, 2-4 Hibikino, Wakamatsu, Kitakyushu 808-0196, Japan

*manish.iitp12@gmail.com; shyam@life.kyutech.ac.jp

Abstract

Solution processable conjugated polymers (CPs) possess unique molecular structure in terms of extended π-conjugation in combination with quasi 1-dimensionality, which impart them an inherent tendency of molecular self-assembly ultimately controlling their optoelectronic properties. Shot range molecular ordering and long range macroscopic orientation are two different but interdependent phenomena, which should be optimized depending on the nature of electronic devices (planer verses vertical). Judicious control of macromolecular orientation and conformation-assisted morphology of CPs are the key to decide and control the anisotropic charge transport in organic field effect transistors (OFETs). Present review focuses on the different solution based approaches for thin film fabrication developed in the last two decades aiming towards controlling the film morphology along with macroscopic orientation of CPs. It summarizes the course of understanding of the various techniques utilized for controlling the molecular ordering and macroscopic orientation in the thin film of CPs in order to correlate the device performance and anisotropic charge transport in OFETs. Systematic organization of topics, critical analysis on their progress and improvisations along with the current state-of-art for each techniques have been discussed in detail. Apart from the commentary on pros and cons of the various techniques, review has been summarized along with future prospects necessary for the further development in the area of next generation flexible electronics.

1. Introduction

Silicon based electronic devices has been highly successful and is the backbone of today's electronic circuits in myriad forms. Amongst different electronic devices, simple and elegant field effect transistors (FETs) has been seamlessly imbibed in our lifestyle in an undistinguishable manner. However, a new category of electronic devices utilizing organic semiconductors has gained appreciable attentions in the past three decades leading to the extensive research aiming towards the practical realization flexible electronics.[1–6] Effort in this direction was geared after the development of new solution processable conjugated polymers (CP) as active semiconductor element and new device fabrication methods. The solution processability, enormous possibility of molecular engineering and control of solution rheology in CPs imparted them an edge over small molecule organic semiconductors for realizing the aim of next-generation low cost flexible electronics. Controlling the thin film morphology assisted by molecular self-assembly of the CPs plays a key role in deciding the performance of the organic electronic devices.[7–9] Owing to inherent quasi 1-dimensional nature of CPs, transport properties can be easily enhanced if the main-chain backbone can be oriented in a particular one direction, which can lead to anisotropic charge transport. Such orientation methods to induce anisotropic charge transport is of interest for realizing the dense arrays of Organic Field Effect Transistors (OFETs) with least possible parasitic current interfering with adjacent OFETs by adjusting the geometry of the electrodes. In general, the large-scale orientation of CPs can be understood in two ways: a) the preferred alignment of main-chain of CPs with respect to substrate plane and b) the length scale of this alignment. The preferred alignment of the CPs on the substrate is crucial as this impact the transport performance significantly, whereas length scale of orientation is highly important for realizing the dense array of devices for practical application.[10,11] A number of reviews have been dedicated to the on the

description of charge transport mechanism of OFETs based on solution processable CPs by many researchers, which can be precisely referred to have more in depth understanding.[5,12–15] In this review, our focus has been centralized to review different types of orientation methods that have been adopted in the processing of thin films utilizing CPs to orient them macroscopically along with the recent developments in the last 10 years. In order to grasp the content and related discussion pertaining to the molecular orientation and their implications on the device performance, introduction about the basic conformations that CPs adopt in their thin film along with their characterization techniques have been discussed in the beginning.

As shown in the schematic **Fig. 1,** polymer backbone can take any of the three different preferential arrangements such as edge-on, face-on and end-on. In edge-on orientation, the conjugated backbone axis and π-stacking axis lie in parallel to the plane of the substrate, whereas alkyl-stacking direction lies normal to the substrate plane. Contrary to this, face-on orientation has conjugated backbone axis and alkyl-stacking axis parallel to the substrate plane with π- π stacking axis normal to the plane of the substrate. It is well known that high carrier transport is believed to occur along the conjugated backbone direction and in π-stacking direction, whereas alkyl side chains act as insulating barriers leading to low carrier mobility in alkyl stacking direction.[16] In this regard, edge-on orientation is highly suitable for OFETs concomitantly leading to high in-plane transport, whereas face-on and end-on orientation is desirable for devices needing high out-of-plane transport such as organic photovoltaics (OPVs) and light emitting diodes.[7,17,18] In the literature, very little is reported about the end-on orientation of CPs and their related transport, where polymer backbone direction is normal to the substrate,[19–21] which can give the highest out-of-plane transport properties in CPs and are most favorable conformation for the OPVs as demonstrated by Tajima group.[22–24]

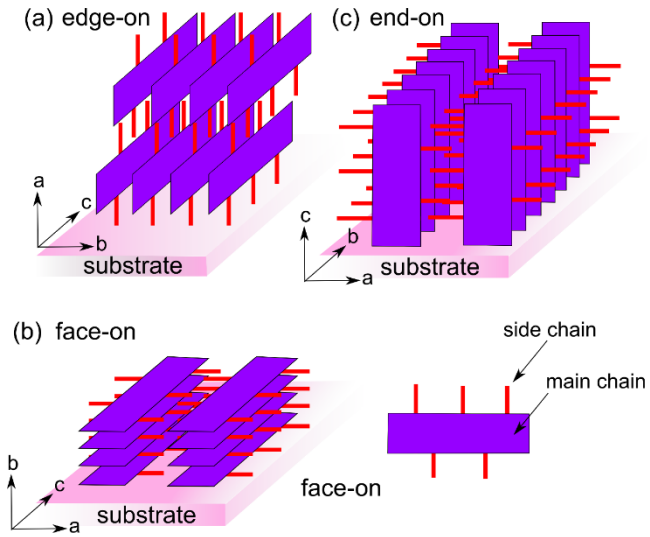

Fig. 1. Schematic representation of different orientations in P3HT on substrate. Edge-on (a), Face-on (b) and End-on (c).

1.1. Quantitative estimation of the orientation

Polarized ultraviolet-visible (UV-Vis) electronic absorption spectroscopy and photoluminescence spectroscopic measurements has been widely used to determine the orientation intensity and referred as optical dichroic ratio (DR). As shown in **Fig. 2**, the oriented thin films on glass/quartz substrates is placed in between the source and detector. With change in the angle of polarizer, magnitude of the absorbance keep on changing reaching maximum followed by a decrease, which reflects that the polymer chains are aligned in a particular direction. In this case, the peak intensity of the absorption spectra is maximum when polarized light wave oscillate parallel (0°) to orientation direction and minimum, when it is perpendicular. Further, DR_{Abs} through polarized absorption is described as $A_{\parallel}/A_{\perp}$, where $A_{\parallel}$ and $A_{\perp}$ are the absorption intensities for the lights polarized parallel and orthogonal to the orientation direction of the CPs, respectively. The transition probability is maximized with transition moment of the macromolecules lying parallel to the electric vector of the light. At the same time, DR of photoluminescence (DR_{PL}) is described

as $I_{\parallel}/I_{\perp}$, where $I_{\parallel}$ and $I_{\perp}$ are the emission intensities of parallel and perpendicular to the orientation direction, respectively. Since most of the reported DR values are carried out utilizing polarized UV-Vis absorption spectroscopy, therefore, DR_{Abs} in this review will be referred as DR.

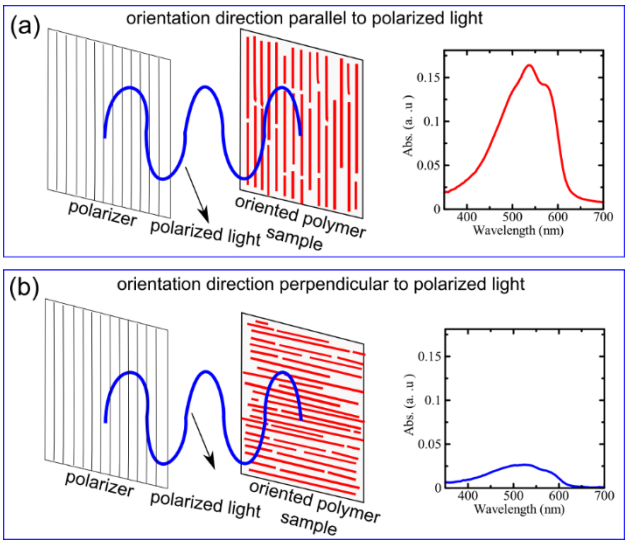

Fig. 2. Schematic representation of polarized absorption spectroscopy.

1.2. Determining the orientation qualitatively

Although the orientation intensity of the thin films of CPs is determined quantitatively by the polarized absorption spectroscopy; however, X-ray diffraction (XRD) based measurements is an essential tool to know the microstructure of thin-films as they yield in-depth information on crystallinity, molecular packing, their orientation and defects.[25–27] Therefore, this technique is very often used to analyze the microstructure of the films. If the films are comprised of domains consisting of un-oriented or randomly oriented CPs, then the XRD pattern coincides to that of crystalline powder.[25] The XRD techniques for CPs has been already reviewed elsewhere in details,[28] however, it has been exemplified considering the unit cell of the conjugated polymer to be orthorhombic for easy understanding. The schematic of the typical texture of grazing angle incidence X-ray diffraction (GIXD) with 2-D detector is shown in the **Fig. 3**.[29] If the *a*-axis is

highly stacked and oriented parallel to the substrate then its peaks will appear along the q_z direction, therefore, the appearance of *b*-axis and *c*-axis will be in plane of the substrate. For such thin films, the appearance of the (*h00*) peaks will appear along the q_z (out-of-plane XRD pattern) and only peak corresponding to (*0kl*) will appear along the q_{xy} (in-plane XRD pattern). Opposite to the former case, if a-axis lie in plane of the substrate the (*h00*) peaks will appear along the q_{xy} direction and (*0kl*) peaks along the q_z direction. However, if the films' orientation of these axis is not ideal, such that some fractions of the film are misoriented in comparison to the majority, their corresponding peaks starts to appear along both q_z and q_{xy} in the XRD pattern. For the same, GIXD measurement pattern is widely used to probe the orientation of CPs in the thin film deposited on any substrate. Due to semi-crystalline nature of the CPs, these measurements are usually conducted with synchrotron light sources with 2-D detector; however, with advanced X-ray diffractometer, these XRD patterns can be obtained by recording the pattern through out-of-plane θ–2θ measurement and in-planes XRD pattern through ω–2θ detector moving in plane of the substrate.[30–32]

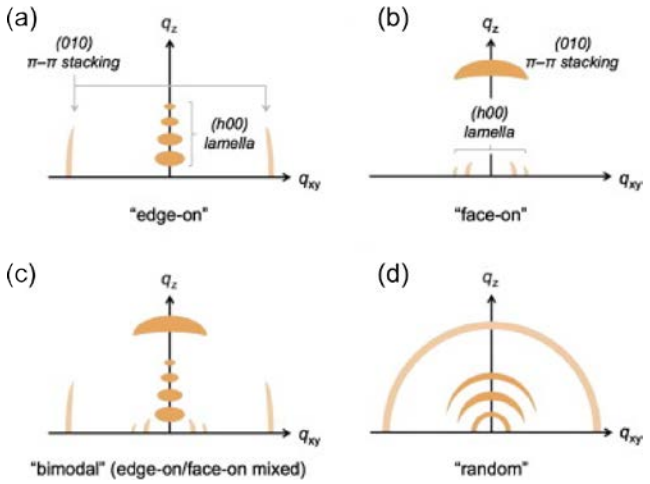

Fig. 3. Typical textures that can be observed in the grazing incidence wide-angle X-ray diffraction (GIXD) with a 2D detector, which corresponds to edge-on (a), face-on (b), bimodal (coexistence of edge-on and face-on) (c), and random orientation (d). (Reprinted with permission from 29. Copyright 2015, Elsevier.)

All of these XRD based techniques are extremely powerful but their demerits include the special resolution and they don't provide enough information about amorphous regions formed with in the film. Usually, X-rays are interface selective and penetrate through the entire thickness of the CP's film. In these terms, Near-edge X-ray absorption fine structure spectroscopy (NEXAFS) allows the determination of backbone orientation of CPs with respect to the surface and probes the top few layers.[33]

A number of methods to induce orientation in CPs have been demonstrated in the recent past. These orientation methods can be broadly classified into three categories such as **1**) use of shear forces to induce orientation by mechanical means, **2**) utilizing orientation ability of CPs in solution phase and **3**) utilizing the orientation ability of the substrate to align the CPs as a guest on the substrate. In this review, efforts have been directed to include all of the major methods under first two categories to orient CPs aiming towards their application for anisotropic charge transport especially in OFETs. First section mainly deals with orientating the macromolecules by means of the external mechanical forces, while later section includes molecular self-assembly driven orientation utilizing solution phase of the CPs. In this category, self-alignment of CPs is either controlled by driving the solution meniscus on a solid substrate or utilizing the viscosity of liquid substrate for controlling the orientation. Third category, utilizing the orientation ability of the substrate to align the CPs as a guest on the substrate has been already reviewed by Brinkmann group in details and not much progress have been done after that.[10]

2. Orientation by external mechanical forces

2.1 Friction Transfer Method

Friction transfer method was originally developed by Wittman and Smith to prepare oriented layers of poly (tetrafluoroethylene) and many researchers have frequently utilized these oriented layer for assisting the orientation of the guest materials.[34–38] Later on, Yase and other groups extensively used this method to prepare highly oriented thin films of many CPs such as poly(9,9′-dioctyl-fluorene) (PFO), poly(2,5-dioctyloxy-1,4-phenylenevinylene), poly(3-alkylthiophenes), poly(dimethylsilylene), poly(p-phenylene), poly[benzo[1,2-d:4,5-d′] bisthiazole-2,6-diyl(3′,4,4″,4‴-tetradodecyl[2,2′:5′,2″:5″,2‴-quarterthiophene]-5,5‴-diyl)] (PTB).[29,31,39–41] One of the beauty of this method lies in the fact that insolubility of materials does not pose any constraints for the fabrication of the thin oriented films. In this method as shown schematically in **Fig. 4**, a polymer is first compressed with high pressure in to a pellet under vacuum and then either the pellet or the substrate (depending on the setup) is slide with a constant speed under certain pressure, which can be generated by putting different loads on the pellet-holder. The temperature of the plate and substrate has to be optimized depending on the nature of polymer under investigation. This direct casting of polymer from the solid phase to oriented thin films is very advantageous as it makes easy to orient insoluble as well as poorly soluble polymers.[42,43] Recently, our group has also prepared large area thin films of poly[2,5-bis(3-alkylthiophen-2-yl)thieno[3,2-b]thiophene] (PBTTT) thin films using friction transfer method and probed the uniformity in thickness and optical anisotropy by our newly developed 2D positional mapping system.[44] In this work it was clearly demonstrated that friction transferred thin films are highly uniform with appreciably good optical anisotropy having DR value reaching up to 10. Nagamatsu and coworkers have fabricated highly oriented thin films of P3HT and poly(3-dodecylthiphene)

(P3DDT) with DR of 10-100 and order parameter (O) close to unity as can be seen in Fig 4 (b). They have demonstrated that orientation direction of the conjugated backbone was parallel to the drawing direction and extent of such a high orientation was confirmed by in-plane GIXD. GIXD profile perpendicular to the orientation direction resulted in appearance of a series of pronounced diffraction peaks (*a00*) corresponding to the stacking of the alkyl side chains (*a*-axis) and peak (*010*) corresponds to π-stacking (*b*-axis), thereby adopting face-on orientation. The absence of the (*a00*) and (*010*) peaks parallel to drawing direction clearly demonstrated that both of the alkyl side chains and π-stacking direction are perpendicular to the conjugated backbone. Very interestingly, this highly oriented film has shown remarkable full width at half maximum (FWHM) of 10° for (*100*) and (*010*) reflections. For the OFETs fabricated with this method utilizing P3DDT, the hole mobility anisotropy ($\mu_{\parallel}/\mu_{\perp}$) of 8 was found.[45] Although in most of the CPs oriented by this method adopts face-on orientation, it has been demonstrated that poly(3-butylthiophene) (P3BT) adopts edge-on orientation, which was attributed to the presence of relatively short alkyl side chains.[46]

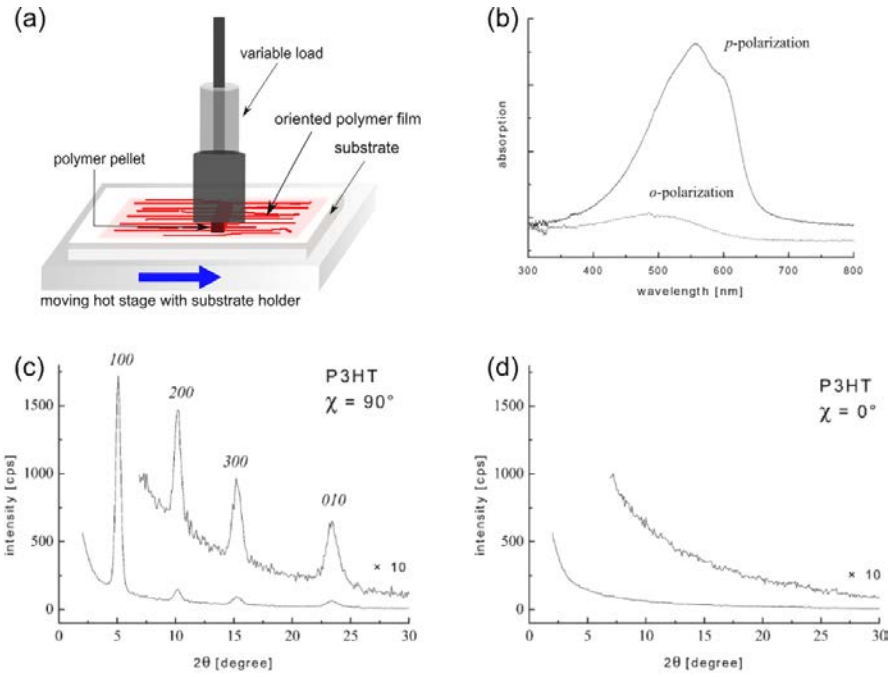

Fig. 4. (a) Schematic diagram for friction transfer. Polarized UV-vis. absorption spectra of the friction-transferred P3HT (b), GIXD pattern of friction-transferred P3HT with scattering vector Q perpendicular to sliding direction (c) and parallel to sliding direction (d). (Reprinted with permission from 30. Copyright 2003, American Chemical Society.)

Later on, Hosakawa et al. has also utilized this method to prepare highly oriented thin films utilizing poorly soluble polythiophene derivative (PTB) with DR of 8 as shown in **Fig. 5**.[43] Difference in the vibronic profile of polarized electronic absorption was due to the different kind of conformation that PTB adopted in the thin films fabricated at 100°C and 240°C (Fig. 5 a, b). The GIXD pattern at 100°C showed a series of arc related to (*h00*) reflections along q_y. In contrary to this, (*h00*) peaks appeared along q_z direction with films prepared at 240°C. These results demonstrated that there was a transformation in the molecular orientation from face-on to edge-on, when the temperature of the substrate increased from 100°C to 240°C and a mixture of both the orientation at intermediate temperatures. Interestingly, this result demonstrated FETs with very high $\mu_{\parallel}/\mu_{\perp} \sim 10^4$ in pure face-on oriented films and $\mu_{\parallel}/\mu_{\perp} \sim 10^1$ with edge-on oriented films. These results demonstrated the significance of edge-on orientation for high in-plane charge carrier

transport, which is crucial for the planer devices like OFETs. The merit of this method lies in the ease of film formation with different molecular orientation (face-on and edge-on) without using harmful organic solvent. This method is highly suitable for achieving orientation in insoluble CPs but high-temperature annealing to achieve orientation is not suitable for flexible substrates. At the same time, this method is not suitable for the multilayers of oriented films and physical damage to the underlying substrates is another bottleneck especially for their application in ultrathin OFETs. Fabricating pellet of CPs limits the use of this technique at laboratory scale as more than 300 mg of CPs are required to start the film fabrication.

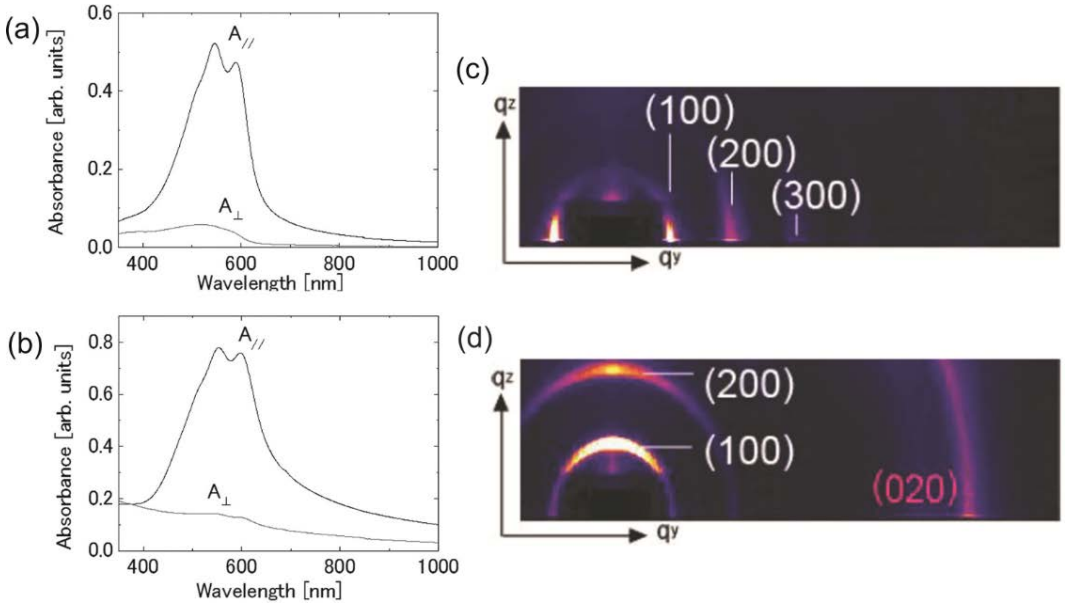

Fig. 5. Polarized electronic absorption spectra of friction-transfer PTB films prepared at (a) 100°C and (b) 240°C with their respective GIXD pattern at 100°C (c) and 240°C (d). (Reprinted from Ref. 43, with the permission of AIP Publishing.)

2.2 Mechanical Rubbing

Mechanical rubbing method for imparting the molecular orientation is being used since long time. Utilization of this method for the alignment of CPs dates back to 1987, when Kanetake and coworkers oriented the vacuum deposited thin films of polydiacetylene.[47] Later, Hamaguchi and Yoshino prepared oriented thin films of poly(2,5-dinonyloxy-1,4-phenylenevinylene) for polarized light emission and subsequently applied to to orienrt the poly(3-alkylthiophenes) (P3ATs) exhibiting the polarized fluorescence.[48,49] They have also demonstrated the alkyl chain length dependence on DR in the rubbed P3ATs and dependence of rubbing cycles as a function of the alkyl length in P3ATs. The effective orientation of fluorescent dyes in composite films with P3ATs have also been demonstrated.[49] Rubbing the polymer films (especially polyimide) has been used to prepare oriented thin films serving as a template for alignment of liquid crystals in liquid crystal displays.[50–52] In the mechanical rubbing, orientation in the polymer is achieved by a rubbing rotating cylinder (covered with cloth) at a constant speed and pressure as schematically illustrated in the **Fig. 6**. Later, Bolognesi and coworkers utilized this method to increase the orientation of poly[3-(6-methoxyhexyl)thiophene] by the combined effect of rubbing and annealing utilizing liquid crystalline (LC) self-organization.[53] Heil at al. investigated the influence of rubbing in P3HT and its related charge transport anisotropy in OFET and demonstrated the DR of 5.1.[54]

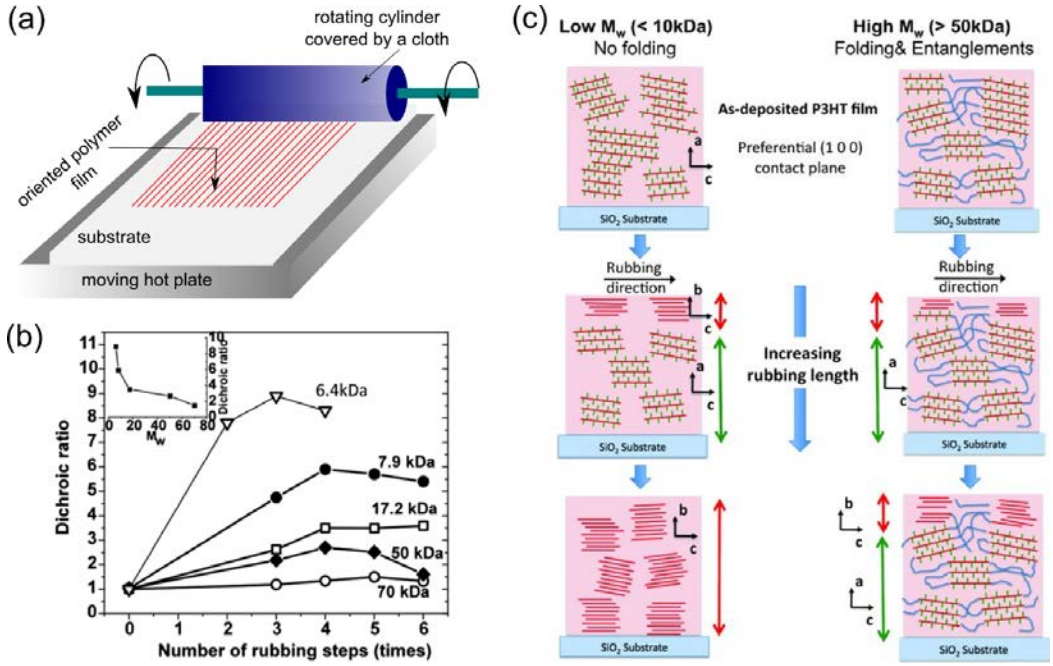

Fig. 6. (a) Schematic diagram for mechanical rubbing and (b) evolution of the DR measured at 550 nm for rubbed P3HT films corresponding to different molecular weights in the range 6.4–70 kDa as a function of the number of rubbing cycles. The inset represents the highest observed dichroic ratio of the rubbed films as a function of molecular weight (M_w). (c) Schematic illustration of the change of P3HT crystallite orientation in the rubbed films with increasing rubbing length for the case of non-folding chains (M_w< 10 kDa) and strongly entangled and folded P3HT chains (M_w > 50 kDa). (Reprinted with permission from 55, copyright 2011 John Wiley & Sons.)

Effect of the mechanical rubbing was further extensively investigated for in-depth understanding of the molecular orientation by Brinkmann group utilizing a number of CPs such as P3HT, PBTTT, poly{[*N*,*N*'-*2*-yl(2-octyldodecyl)-1,4,5,8-naphthalenedicarboximide-2,6-diyl]-alt-5,5'-(2,2'-bithiophene)} (P(NDI2OD-T2)) and PFO etc.[55–58] Hartmann et al. showed the dependence of induced orientation in P3HT by mechanical rubbing as a function of molecular weight and rubbing cycle. As shown in Fig. 6 (c), high in-plane orientation was obtained with the polymers with relatively lower molecular weight $M_w \leq 7.9$ kDa of P3HT, which keeps on decreasing with increase in the M_w. Impact of rubbing cycle on the orientation of different molecular weight indicated that sequential increase in rubbing cycles effectively increases the

orientation, however, this was more effective for the low molecular weight polymers. Electron diffraction (ED) measurement indicated the changes in the preferential alignment of polymer chains parallel to the rubbing direction propagating to the entire thickness of the films by increasing the rubbing cycles, and there was flipping of the polymer orientations from the edge-on to face-on.[55] They have shown that transport anisotropy in P3HT was consistent with characterization results with the maximum value of $\mu_{\parallel}/\mu_{\perp}$ for low molecular weight samples and vice-versa. Subsequently, they demonstrated that high temperature mechanical rubbing of the polymers as a function of their molecular weights in case of P3HT, PBTTT, PFO and P(NDI2OD-T2).[58,59] As shown in **Fig. 7**. GIXD results for high temperature rubbing with of P3HT and PBTTT showed (*h00*) reflections (h =1−3) for qi||R direction and these reflections are absent for qi⊥R indicating face-on oriented domains for both the polymers. For qi||R, the presence of edge-on oriented domains was also confirmed in case of PBTTT due to the appearance of (*h00*) reflection along q_z and for P3HT very weak reflection for 100 indicated the presence of a small population of edge-on domains. They showed the FWHM of 14° in the ϕ-scan of 100 reflection of P3HT, very close to Nagamatsu et al. obtained in P3HT by friction transfer method.[30] These results have clearly corroborated that rubbing temperature needed for high orientation critically depends on their molecular weight. This was explained considering the fact that high temperature rubbing continuously creates fluidity in alkyl side chains concomitantly providing freedom to backbones by dis-entangling from neighboring macromolecules.

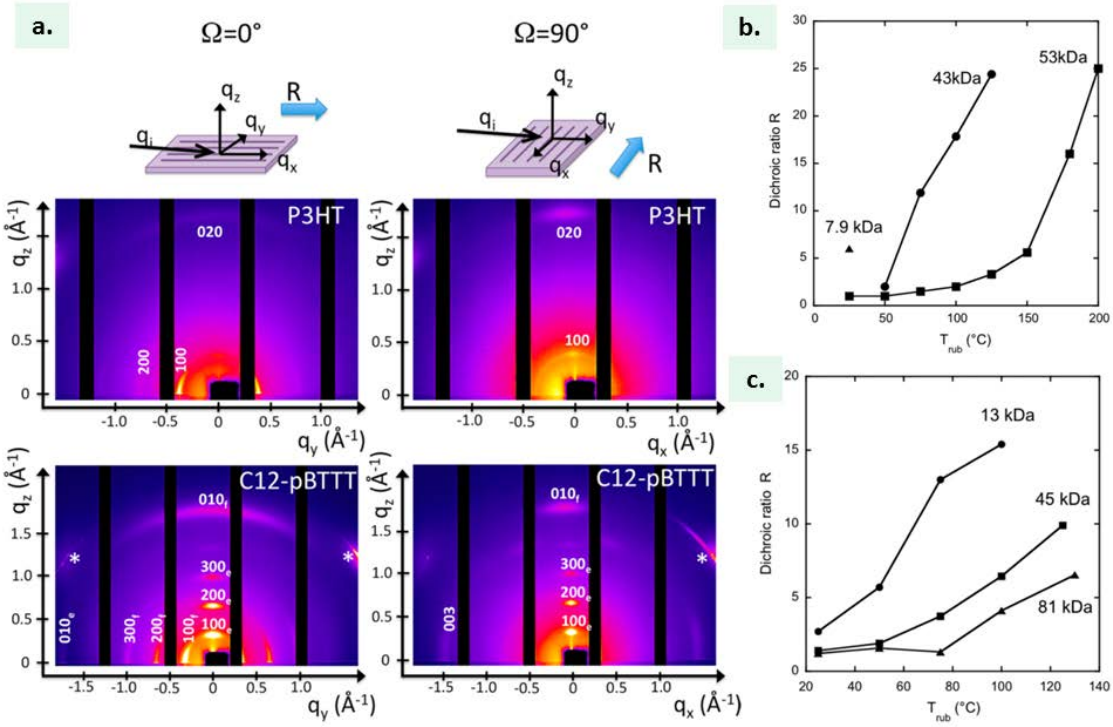

Fig. 7. (a) GIXD 2D maps obtained for rubbed films of P3HT (43 kDa, T_{rub} = 180 °C), C12-pBTTT (45 kDa, T_{rub} = 100 °C). Incident X-ray beam oriented parallel (Ω =0°) and perpendicular (Ω =90°) to the rubbing direction R as illustrated in the top sketches. In the case of C12-PBTTT, the main reflections are indexed with labels corresponding to the population of face-on and edge-on domains. The asterisk indicates reflections from the Si (100) substrate. T_{rub}-dependence of the dichroic ratio at 605 nm for P3HT (b) and C12-PBTTT (c) thin films rubbed as obtained for different molecular weights. As a mean of comparison, the DR of a P3HT 7.9 kDa sample rubbed at 25 °C is shown in part (b). (Reprinted with permission from 58. Copyright 2014, American Chemical Society.)

Further, effect of doping of polythiophene thin films prepared by mechanical rubbing with 2,3,5,6-Tetrafluoro-7,7,8,8-tetracyanoquinodimethane (F4-TCNQ) on the crystal structure and charge transport was also investigated by the same group.[60] Their ED results indicated a moderate expansion in distance between the side-chains due to the presence of the guest F4-TCNQ molecules but resulted in to reduced π-π stacking distance. Contrary to this, there was enhanced π-π stacking in the case of PBTTT resulting into the conformation change from face-on to edge-on upon doping with F4-TCNQ in its rubbed thin films. Although, such a conformational change

was observed only when the film was annealed to its LC phase transition temperature. It was also observed that the overall charge transport anisotropy in terms of conductivity (σ) increases with mild doping was mainly due to the enhancement along the rubbing direction (from $\approx$5 to 22 $\pm$ 5 S/cm), which increases as a function of doping.[59] It can be explained considering the fact that sheer forces from the cylinder are applied normal to the film plane, therefore, mechanical rubbing induces face-on orientation and the possibility to adopt edge-on orientation was induced by annealing at high temperatures.[56] Such a face-on orientation is suitable for out of plane transport as π-π stacking direction is out-of-plane. Recently, Saito group have shown considerable enhancement in the out-of-plane mobility in rubbed films of P3AT.[61,62]

2.3 Roll Transfer Method

Roll transfer is another method of orienting macromolecules developed by Naito group,[63,64] which seems to be inspired by the mechanical rubbing technique as shown in **Fig. 8**. The only difference lies in the fact that films is first spin-coated on the polydimethylsiloxane (PDMS) substrate followed by its transfer on to the desired substrate. The substrate temperature plays an important role in this method because the polymer first goes in to LC phase, where backbone chain melts and renders freedom for their alignment while transferring. Especially, orientation in the LC phase bearing solution processable conducting polymer poly(3,3‴-didodecylquarterthiophene) (PQT) prepared by this method was demonstrated to be the edge-on leading to higher mobility along the orientation direction with $\mu_{\parallel}/\mu_{\perp}\sim$ 8. Later, it was found that mobility in oriented PQT are higher along the 30° from the orientation direction.[64] Although this method has not been adopted widely and can be applicable to only those materials, which show thermotropic LC properties. It is also worth to mention here that this observed high mobility at 30° is a specific case for this polymer using this method and cannot be generalized for every CPs and orientation methods.

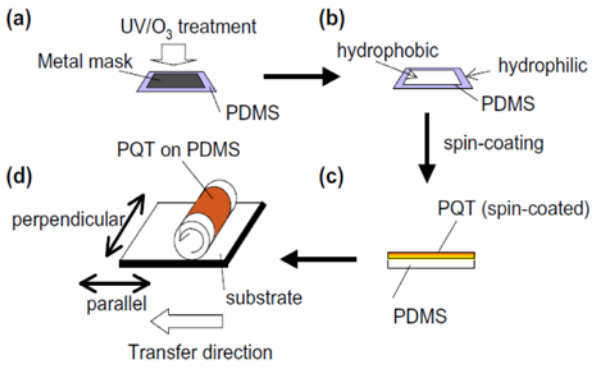

Fig. 8. Schematic diagram of roll-transfer printing. Preparation of a peripheral hydrophilic region on the PDMS stamp (a) and (b), spin coating the PQT film onto the PDMS stamp (c) and Roll-transfer printing of the PQT film onto the substrate (d). (Reprinted with permission from 63. Copyright 2011, Elsevier.)

2.4 Strain Alignment

Stretching the deposited layer of CPs on flexible substrates such as polyethylene and PDMS can lead to the alignment of the CPs in the direction of the stretching. This method was introduced by Dyreklev et al., where they demonstrated that stretching two times to that of the original length of the deposited poly 3(4-octylphenyl)-2,2′-bithiophene on polyethylene leads to orientation in the main chains leading to a DR_{PL} of 2.4.[65] Later, O'connor et al. obtained high orientation in P3HT by straining the deposited film on PDMS with DR of 4.8.[66,67]

As shown in the **Fig. 9**, extent of induced DR by thus method was directly proportional to the applied strain. The GIXD results exhibited a change in the crystallite orientation of the backbones from edge-on to face-on and schematically summarized in the Fig. 9. Their phi-scan of 100 reflection revealed the FWHM of 23°. The field effect mobility increases with an applied strain reaching maximum in the case of orientation parallel to the direction of strain and lowest for the perpendicular orientation with maximum $\mu_{\parallel}/\mu_{\perp}$ of 9.

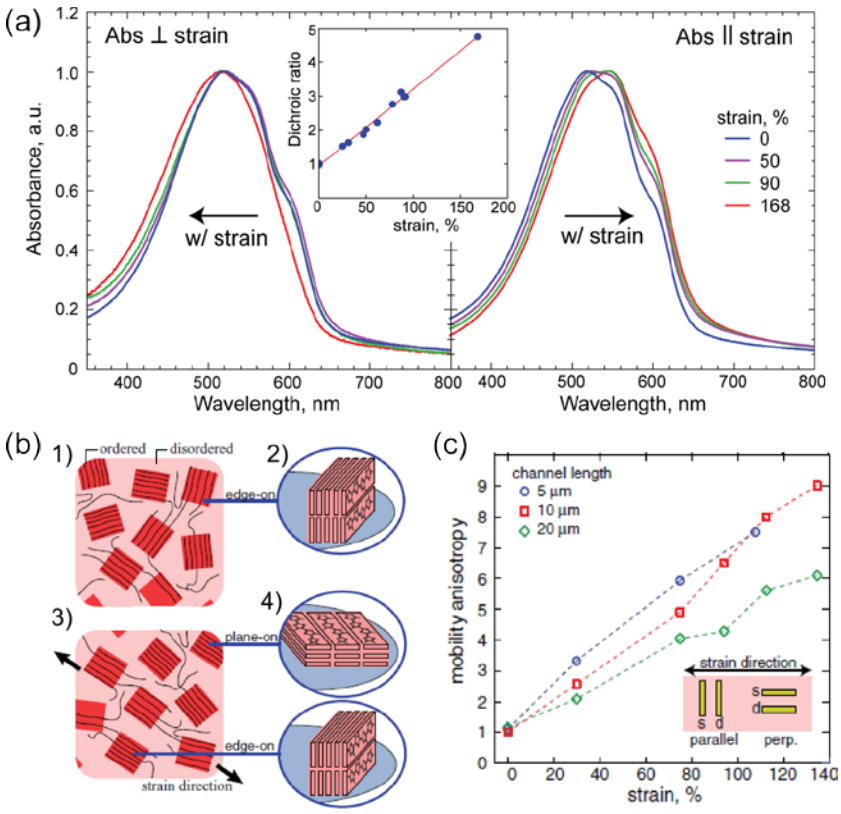

Fig. 9. (a) Normalized absorbance of P3HT films under varying levels of strain. All absorbance curves are normalized by the maxima of the spectra. Left: absorbance with light polarized perpendicular to the strain direction. Right: absorbance with light polarized parallel to the strain direction. Inset: dichroic ratio of the P3HT films over a range of strains, with a linear fit to the data. (b) Schematic view of the strain P3HT film 1) Top view of a small portion of the polymer illustrating the semi-crystalline nature of the polymer of randomly oriented crystals (dark red) within an amorphous matrix (light red). The black lines represent the polymer backbone 2) Oblique view of the polymer stacking direction illustrating an edge-on morphology, which is observed for an unstrained fi lm. 3) Under strain, the polymer crystals are reorienting with the polymer backbones aligning in the direction of applied strain, while the amorphous material remaining highly disordered. 4) Oblique view showing the increasing level of plane-on P3HT polymer in the alignment direction, while the crystals with the backbone initially in the direction of applied strain remaining edge-on, (c) mobility anisotropy of strain aligned P3HT films for transistors with 5, 10, and 20 μ m channel lengths. (Reprinted with permission from 66. Copyright 2011 John Wiley & Sons.)

Later, Xue et al. utilized this method to orient PBTTT with large ordered domains. Since PBTTT films are very brittle and crack under the strain of 3%, they utilized its LC behavior and applied the strain by keeping the films slightly above the hot plate at LC temperature, where side

chains become characteristically liquid-like.[68,69] Direction of the orientation was parallel to the strain direction with DR of 2.2 for as cast film when strained up to 60% and there was an increase in the DR upon the further annealing of the films as shown in **Fig. 10**,. They also reported the problem existing with the dewetting of film and its related issue in strain alignment shown in the AFM image. The GIXD results showed no change in the crystallite orientation and films exhibited edge-on orientation before and after strain alignment. Field effect mobility of the strain-aligned films was found to be higher in the direction parallel to the strain as compared to that of perpendicular one. Moreover, they demonstrated the highest charge carrier mobility for this class of polymer reaching 1.67 $cm^2V^{-1}s^{-1}$ with platinum source/drain electrodes and channel length of 5 µm. Although strain alignment was reported to be very effective and easy strategy to prepare oriented films but preparing large area thin oriented films seems to be difficult for large-scale manufacturing. The problems existing with the film breakage in the case of crystalline materials limits its wide spread use and can only be applicable for low crystalline materials.

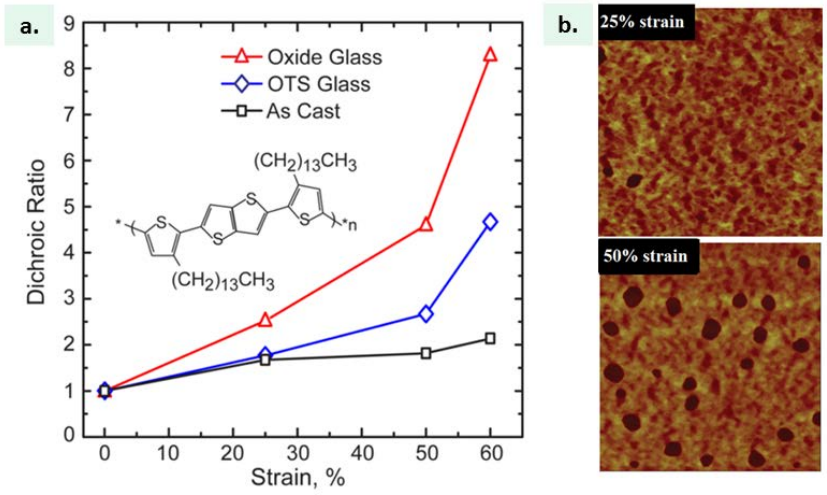

Fig. 10. Change in the DR taken at 550 nm for PBTTT films prepared on oxide glass (annealed at 180 °C), OTS treated glass (annealed at 180 °C), and as- cast film plotted as a function of applied strain (a). AFM images taken under 25% strain and 50 strain at dimension 5µm×5µm. (Reprinted with permission from 69. Copyright 2015, American Chemical Society.)

2.5 Film Compression at surface of ionic liquid

This method to orient CPs with high phase transition temperature was introduced by the Takeya group. They demonstrated that compressing the casted thin floating films on liquid substrate (ionic liquid) in one direction induce orientation in CPs such as PBTTT, poly(2,7-bis(3-alkylthiophene-2-yl)naphtho[1,2- b:5,6- b′]dithiophene) (PNDTBTC20) and P3HT etc..[70] As shown in the **Fig. 11**, a very dilute solution of the polymer was applied on the ionic liquid (kept at elevated temperature) dropwise to prepare several layers of floating film on the surface of the ionic liquid. The temperature of the ionic liquid was kept at LC transition temperature providing the molecular movement. After the film formation, the film was compressed by a blade at a constant speed of 1mm s^{-1}, which was used orient CPs homogeneously in one direction (perpendicular to compression direction).

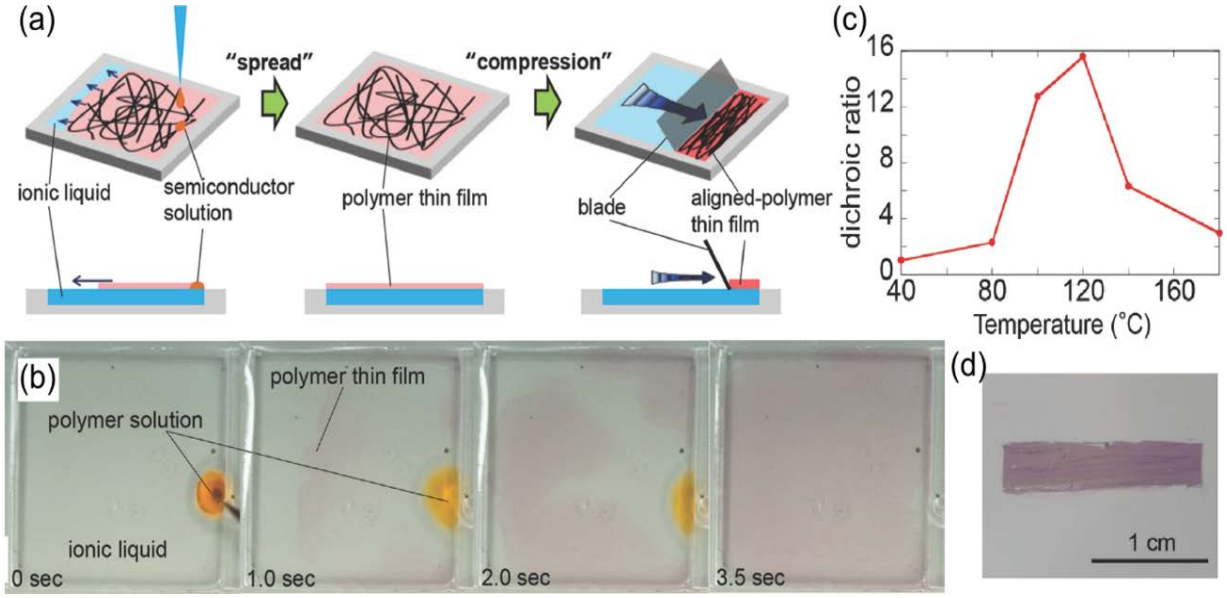

Fig. 11. Schematic Diagram of the spread-and-compress procedure used to prepare thin films (a), polarized UV–vis absorption spectra of the PBTTT film which was compressed at 120 °C (b), Dependence of the dichroic ratio on the compression temperature (c). (Reprinted with permission from 70. Copyright 2014 John Wiley & Sons.)

A perusal of the Fig. 11, clearly reveals that prepared thin films of PBTTT are highly oriented with DR of 15.6, which is the highest value of the optical anisotropy reported for PBTTT. It was demonstrated that DR of PBTTT strictly depends on the temperature of the ionic liquid. At room temperature, they found no orientation. However, the DR increases with the increasing temperature of ionic liquid reaching maximum at 120°C and any further increase in temperatures decreases the DR significantly because of the excessive fluidity of this polymer, thereby making them difficult to be compressed mechanically. Their GIXD results revealed high in-plane orientation with edge-on structure along with some fractions of face-on crystallites too. They reported high field effect mobility in the direction of the backbone orientation with the average electronic anisotropy ($\mu_{\parallel}/\mu_{\perp}$) of ~ 5.3. Interestingly, orientation in CPs without having LC phase transitions such as PNDTBTC20 and P3HT was although observed but DR was found to be relatively lower compared to that observed for PBTTT. This clearly reflect that this method can induce high orientation in polymer having LC phase. Subsequently, they have also oriented thin films of hexadecylsubstitutedcyclopentadithiophene-benzothiadiazole (CDT-BTZ-C16) prepared by this method and reported a very high field effect mobility of 10 $cm^2V^{-1}s^{-1}$.[71] Recently, local alignment of PBTTT films prepared by this method was studied by transmission electron diffraction, which reveals that the polymers are aligned in a gentle winding state with an average radius of curvature ~630 nm.[72] Although not demonstrated, the beauty of this casting method lies is that film fabrication is independent of the substrate and can be characterized on any substrate, which makes it capable of fabricating multilayer films where chemo-mechanical damage does not occur. At the same time, necessity to utilize LC phase to achieve high orientation limits its use for other CPs if the orientation is desired at low temperature.

3. Orientation by alignment ability in solution phase

3.1 Meniscus-Guided Coating Techniques

In the meniscus-guided coating techniques like dip-coating,[9] zone-casting,[73] solution-shearing[74] etc., thin film coating on a substrate is guided by the movement of solution meniscus, which is controlled by the coating head and/or the viscous drag of the polymer solution. The thin film morphology depends on the influence of fluid mechanical phenomena and various flows on polymer aggregation and alignment during coating, as schematically represented in **Fig. 12** (a), detailed discussion can be found elsewhere.[75] Wettability of substrate by the solution is one of the most important requirement for the thin film coating in these methods which depends on surface tension and surface energy of the solution and the substrate respectively and can be controlled by changing solution viscosity and substrate's surface treatment.[76,77] Apart from these, the meniscus guiding speed also plays a vital role to decide the film thickness and microstructural organization.[78–80] Based on fluid mechanical phenomena, the guiding speed can be divided in two regions viz. i) at lower guiding speed i.e. capillary regime and ii) at higher guiding speed i.e., Landau-Levich regime.[75,81–84] At lower speed, the combined effect of solvent evaporation and capillary flow causes the mass flow towards the drying contact line leading to the coffee ring effect.[81] However, at higher speed the film morphology is mainly controlled by the effective viscous drag acting on the meniscus.[83,84] From the perusal of Fig. 12 (b – d), it is clear that the film thickness decreases with increase in the guiding speed in the capillarity regime, however, in Landau-Levich regime it increases with increase in speed and minimum thickness can be obtained at the transition speed. Furthermore it should also be noted that preaggregation in the solution serves as a nucleation site and at the same time. Recent reports have indicated that the occurrence of aggregates in solution helps in macromolecular orientation.[77,80,85,86] Therefore, the selection of

solvent-polymer system is important as poor solvent often causes the polymer aggregate formation in solution, which can also be promoted either by ultrasonication or treating the polymer solution by the mild UV rays.[87–90]

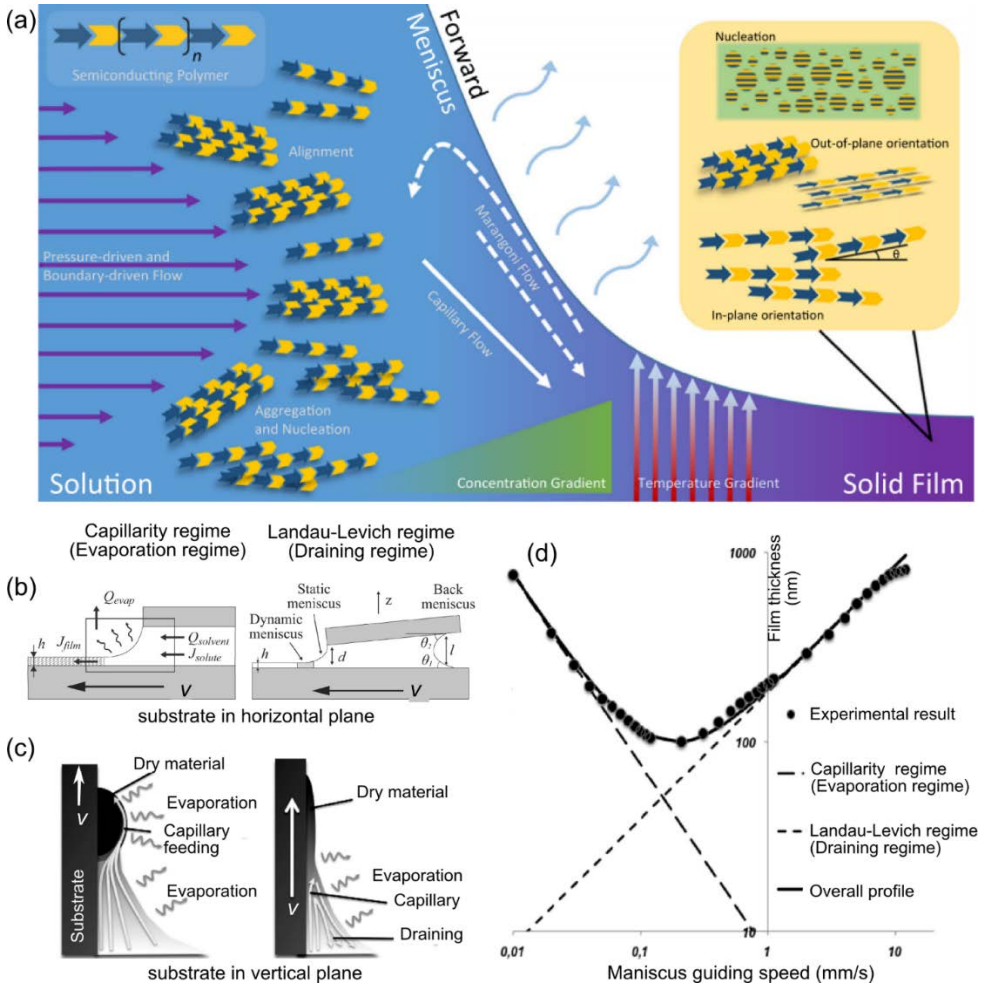

Fig. 12. (a) Summary of flows, gradients, and fluid mechanical phenomena that can influence semiconducting polymer molecules and their resulting microstructure in the thin film. (Reprinted from 75) Schematic illustration for both capillarity and draining regimes involved at low and fast withdrawal speeds, respectively, when substrate and/or meniscus moves in the (b)horizontal plane (Reprinted with permission from 83. Copyright 2009, American Chemical Society.) and (c) vertical plane. (d) Plot of the thickness versus meniscus guiding speed (log-log scale). Experimental points fitted with combined (solid line) independent (dashed line) models for both capillarity and Landau-Levich regimes of film formation represents as coating speed increase, minimum film thickness was obtained at transitioning from capillarity to Landau–Levich regime, where capillarity effect absolutely counterbalances the effect of viscous drag. (Reprinted with permission from 84. Copyright 2010, American Chemical Society.)

3.1.1 Dip Coating: This is one of the oldest technique for thin film fabrication, where a desired substrate is dipped in solution reservoir followed by gentle pulling out for the self-assembly of molecular layer/s, **Fig. 13**(a).[91] Here, the meniscus is translated by the viscous drag caused due to gravitational force and controlled by the factors such as coating speed, solution concentration, viscosity and temperature. There are a number reports pertaining to the improved thin film morphology of dip coated films as compared to drop casted or spin coated ones.[92–94] Mullen group first demonstrated anisotropy in dip coated thin films of cyclopentadithiophenebenzothiadiazole copolymer (CDT-BTZ), where they reported around twofold enhancement in hole mobility in the dip coated films (1.4 $cm^2V^{-1}s^{-1}$ with $\mu_{\parallel}/\mu_{\perp}\approx2$) compared to that fabricated by spin-coating (0.67 $cm^2V^{-1}s^{-1}$).[9] Later on, same group demonstrated the evolution of anisotropic microstructures and its effect on the charge transport utilizing one of the well explored CPs, PBTTT.[78] This report also provided detailed role of different parameters in the evolution of film's microstructural morphology and emphasized that such films can overcome the need of hydrophobic interface and annealing. By optimizing the pulling speed to 2 μm/s, they found anisotropic fibrous structure in the AFM image as shown in Fig. 13(b). The arrangement of fibrils in the channel of OFET led to record high mobility 1.3 cm^2/Vs with $\mu_{\parallel}/\mu_{\perp}>10$. Interestingly, in the case of PBTTT, the first monolayer showed a 2D microstructure, while the following layers exhibited 1D fibers, Fig. 13(c).

In the following report, for P(NDI2OD-T2), there was no microstructural differences observed between different layers and the reason was attributed to the chemical structure of the CP.[95]

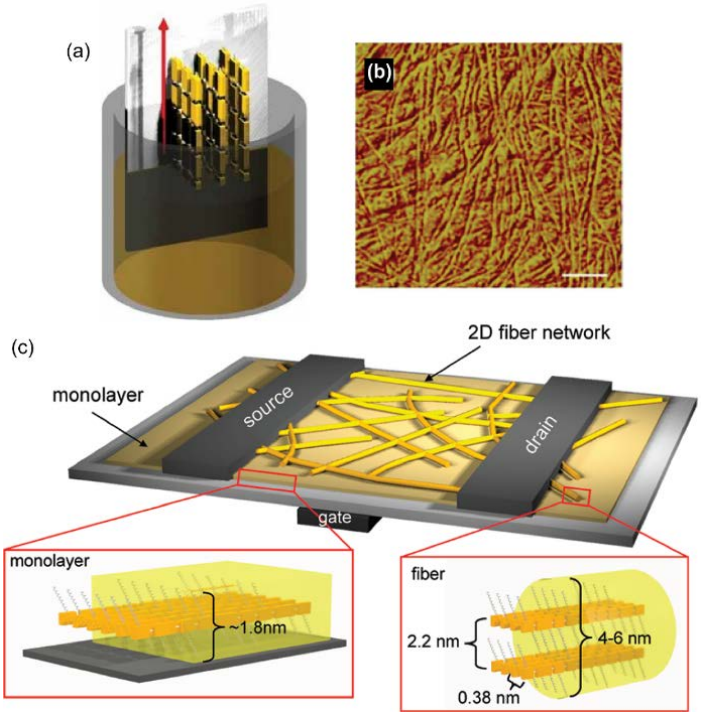

Fig. 13. (a) Schematic illustratio for macromolecular orientation by dip coating. (Reprinted with permission from 9. Copyright 2009 John Wiley & Sons.) (b) AFM image of the uniaxially oriented film dip-coated at 2 μm/s (the scale bar corresponds to 1 μm). (c) Schematic illustration of the molecular organization in the thin film deposited at 10 μm/s. (Reprinted with permission from 78. Copyright 2012, American Chemical Society.)

High solubility of the organic material is essential to prepare thin films by this method, however, certain improvisation in the process has made it possible to coat less soluble organic semiconductors and was termed as two-phase dip-coating.[96] In this method, at first, the extremely dilute ink of the organic semiconductor is cast on the surfactant mixed water followed by few seconds of ageing leading to the formation of aggregates. Then the substrate is dipped to coat the oriented strips of semiconductor thin film. Although this method has been demonstrated only for

small organic molecules, the observed transport property may pave the path of its future application to cast the few partially soluble CPs.

3.1.2 Blade coating: This technique is also known as Doctor Blading or knife-over-edge and main controlling factor in this technique is the relative motion between blade and substrate. Polymer solution acting as a solution reservoir is placed on the desired substrate followed by motion of either blade or substrate. Relative motion between the substrate and the blade wipe out the excess solution leaving a dry (capillarity regime) or wet (Landau-Levich regime) film on the substrate.[75] In this technique, the controlling factors are the separation between blade-edge and substrate, coating speed, and substrate temperature. However, for the fine-tuning of film morphology, other coating parameters such as the surface energy of the substrate and the surface tension/ viscosity of the polymer solution can also be tuned. Although this technique has been utilized for large area fabrication of multilayered fully printed electronics,[97–99] its application to orient the CP has been recently demonstrated by Rechmanies group.[100] They reported about the formation of oriented nanofibrils upon UV-irradiation and enhanced population of the fibrils by aging the UV-irradiated solution. It is worth mentioning here that P3HT forms nanofibrils if irradiated with mild UV rays for ~ 8 mins.[90] They demonstrated drastic differences in orientation characteristics of the blade-coated films prepared with pristine P3HT, UV-irradiated and aged UV-irradiated ones as shown in the **Fig. 14**. Their results revealed that the degree of crystallinity and polymer chain alignment was increased with the aging time of the UV-irradiated P3HT solution. The orientation of the nanofibers was parallel to blade coating direction with polymer chains aligned perpendicular to it.

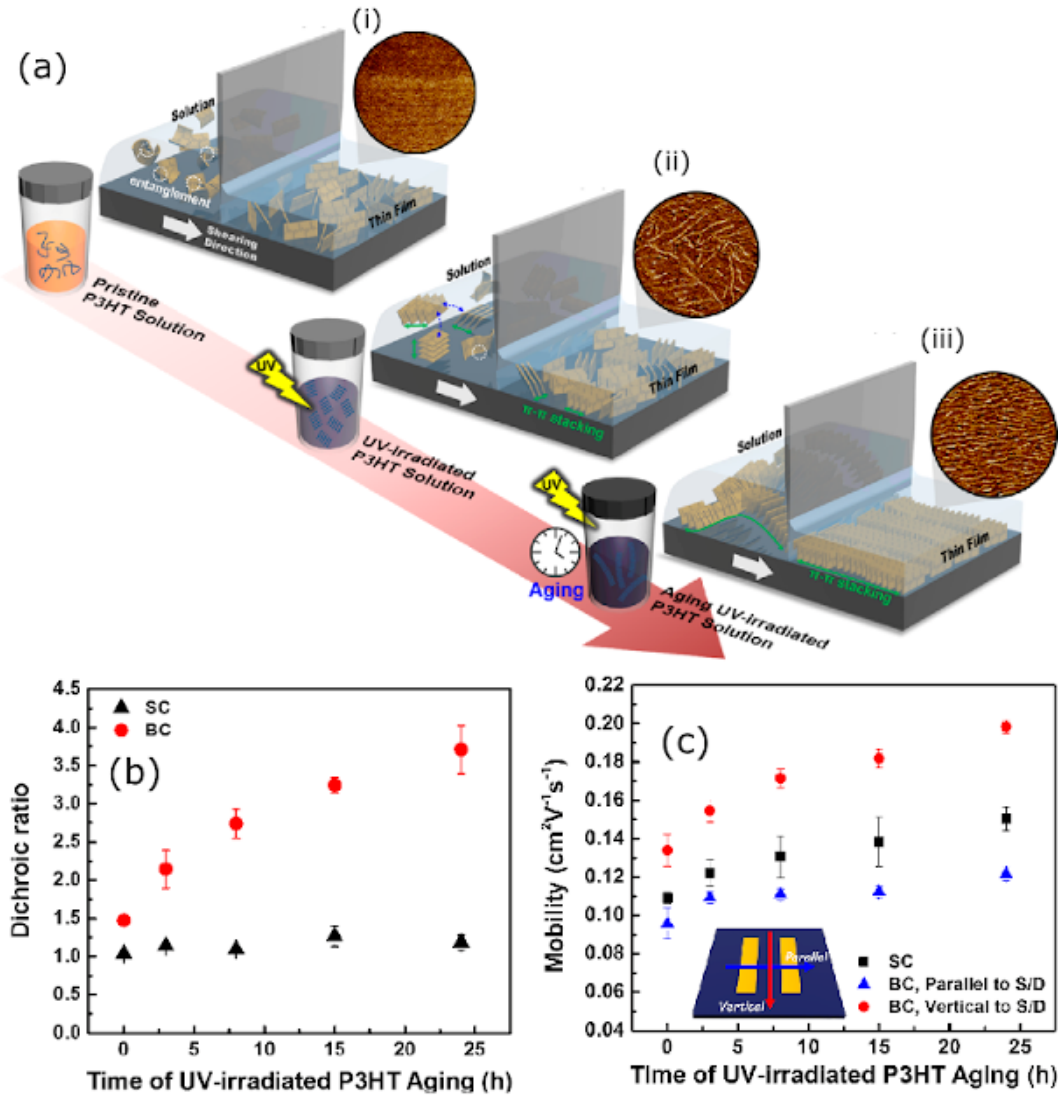

Fig. 14. (a) Schematic illustration of blade-coating process with (i) pristine P3HT (ii) fresh UV−P3HT, and (iii) aged UV−P3HT solutions. (b) Evolution of the dichroic ratio as a function of solution-aging time. (c) Average charge-carrier mobilities of OFETs with active layers deposited by spin coating and blade coating in parallel and vertical directions. (Reprinted with permission from 100. Copyright 2016 American Chemical Society.)

It should be noted that fiber grow along the π-π stacking direction. The DR of the UV irradiated solution were ~ 1.5 and increases continuously with maximum up to 4 after 24 h of aging (Fig. 14 (b)). They reported anisotropic charge transport with high field effect mobility along the orientation direction of the polymer chain in comparison to the fiber direction as shown in the Fig. 14 (c). Although orientation of P3HT nanofibers has been demonstrated using blade coating, use

of this coating method is still limited for preparation isotropic thin films because this blade inspired methods are still not compatible with majority of the CPs until they form nanocrystallites such as nanofibers, nanorods etc.

3.1.3 Solution-Shearing: The name of this technique is derived from the term 'Shear stress' which arises due to a pair of shear forces, which are equal in magnitude but acting in opposite directions at the opposite surfaces.[101,102] In this method, polymer solution is confined between the movable blade surface and the temperature-controlled substrate as shown in the **Fig. 15** (a). During coating, the blade drags top layer of the solution in the forward direction, while the bottom layer is adhered to the substrate and is pulled in the opposite direction. Effectively less exposer of the solution reservoir to the ambient restricts the solvent evaporation to the edges. This controlled drying system has been reported to induce a strained lattice of modified π–π stacking with improved charge carrier transport.[103,104] This technique was initially applied to orient the small molecule organic semiconductors to control their crystal structure leading to significantly higher mobility (up to 11 $cm^2V^{-1}s^{-1}$).[105,106] However, it has been amicably utilized to coat the thin films of CPs also in the recent past. Yabu et al. have utilized this technique to orient P3HT followed by Karakawa et al. who demonstrated its OFET application.[107,108] However, there was only a 2-fold increase in mobility for the films prepared by this method compared to that by spin-coating, which was not much appealing compared to enhancement obtained by this method in the small organic molecules. Reason behind such low mobility for solution sheared CP-thin films was extensively investigated by Bao group,[74] They suggested that the molecular packing of P3HT is not much affected by solution\shearing and comparative electronic absorption spectra revealed the increased fraction of amorphous region at lower shearing speed. However, in the case of CPs with inherent high crystallinity and interdigitated alkyl chain packing such as poly(2,5-bis(thiophene-2-yl)-(3,7-

dihepta-decanyltetrathienoacene) (P2TDC17FT4) and PBTTT, they found increased lamellar spacing in the as-cast sheered films. This represents the formation of metastable structure with disordered stacking of side chains and re-gained the equilibrium structure upon the recrystallization after annealing.[109,110]

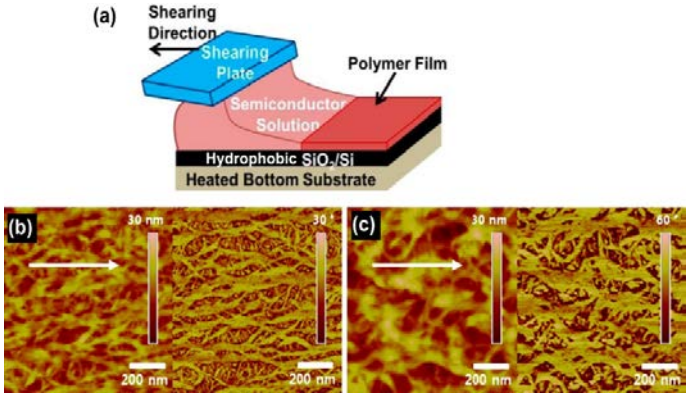

Fig. 15. Schematic illustration of solution-shearing (a). (Reprinted with permission from 74. Copyright 2015 American Chemical Society.). AFM height (left) and phase (right) images of solution-sheared film and annealed at 220°C for PTDPPSe-SiC4 (b) and PTDPPSe-SiC5 (c). (Reprinted with permission from 86. Copyright 2013 American Chemical Society.)

Lee et al. reported enhanced charge transport in the solution-sheared thin films of CPs by introducing pre-aggregation in the polymer solution.[85,86] They observed the improved morphology and reduced π–π-staking distance in the sheared thin film of the ambipolar copolymer diketopyrrolopyrroleselenophene copolymers with hybrid siloxane-solubilizing groups (PTDPPSe-SiC6). Through the synergistic effect of molecular engineering and solution-shearing followed by annealing of the film to 220℃, they were successful to increase average hole mobility (μ_h = 3.48 $cm^2V^{-1}s^{-1}$) by 3-fold and electron mobility (μ_e = 0.97 $cm^2V^{-1}s^{-1}$) by 10-fold. In their following work, they demonstrated the effect of side-chain engineering in the same class of CPs (PTDPPSe-SiC*n*, where *n* = 4 – 6) and emphasized that smaller siloxane-terminated side-chains resulted in denser microstructures with decreased π-π stacking distance and improved device

performance. However, the lower solubility of the copolymer with the smallest side chain (PTDPPSe-SiC4) led to a nonhomogeneous thin film with hampered device performance (Fig. 15 (b). Nonetheless, this fine trade-off between solubility and closely packed lamella/π-π stacking resulted in a high hole and electron mobilities of 8.84 and 4.34 $cm^2 V^{-1} s^{-1}$, respectively for the PTDPPSe-SiC5 films prepared under optimized conditions (Fig. 15 (c). Later, in order to make environment-friendly large scale roll-to-roll fabrication of organic electronic devices, Bao group utilized a mixture of non-halogenated solvents consisted of tetrahydronaphthalene and xylene to cast the solution-sheared thin film of the thiophene-based diketopyrrolopyrrole copolymer (PTDPPTFT4).[111] Xylene exhibiting lower boiling point facilitated polymer aggregation in the solution whereas tetrahydronaphthalene being higher boiling point solvent allowed longer evaporation time and better solubility. With the optimum solvent mixture having 25% xylene, π–π stacking distance of the solution-sheared film (3.62 Å) was smaller than that of equivalent films prepared by spin coating (3.71 Å), which was well reflected in the transport property with the average μ_h of 3.13 $cm^2V^{-1}s^{-1}$ and 2.20 $cm^2V^{-1}s^{-1}$ for solution-sheared and spin-coated films, respectively.

Further progress in this technique was made aiming towards induction of the orientation in CPs by modifying the coating head or the substrates.[79,112,113] Schott et al. reported significantly high DR of ~14 in a donor-acceptor type copolymer poly[[2,5-bis(2-octadecyl)-2,3,5,6-tetrahydro-3,6-diketopyrrolo[3,4-c]pyrrole-1,4-diyl]-alt-(2-octylnonyl)-2,1,3-benzotriazole] (DPP-BTz) by replacing the conventional *rigid coating blade* (glass/Silicon) with a *flexible blade* (solvent-resistant perfluoropolyether (PFPE)) as schematically illustrated in **Fig. 16** (a).[79,114] Pre-aggregation (DPP-BTz/chlorobenzene) in the solution promoted the orientation, as characterized by polarized optical microscopy (POM). Consequently, $\mu_{\parallel}/\mu_{\perp}$ for bottom-contact top-gate OFET

was 3.1 ± 1.6 with lower coating speed and maximum $\mu_{\parallel}$ = 6.7 $cm^2V^{-1}s^{-1}$ was obtained by minor increase in the coating speed, where film quality and macromolecular orientation was balanced, as shown in Fig. 16 (b). Interestingly, temperature dependent band-like charge transport along the polymer backbone orientation was also evidenced. In another report, Shin et al. utilized a shearing blade composed of a PDMS mold patterned with a set of rectangular microgrooves acting as a template to assist orientation in CPs Fig. 16 (c).[112] The optical microscopic image of the sheared films of DPP-based copolymer flanked by thiophene and thienothiophene based donor unit (PTDPP-DTTE) revealed the film morphology with a few micrometer wide micro patterned prisms. They found increase in hole mobility (6.75 $cm^2V^{-1}s^{-1}$) with patterned nanogrooved flexible blade in comparison to that of spin-coated (2.67 $cm^2V^{-1}s^{-1}$) or conventional solution-shearing using a rigid blade (4.53 $cm^2V^{-1}s^{-1}$). The improvement in hold mobility was attributed to increase in contact area between modified-blade and the polymer solution, which causes increased polymer alignment and decrease in π-π stacking distance as confirmed by GIXD measurement. By utilizing nanostructured substrate, Wu et al. demonstrated the controlled macromolecular orientation in the solution sheared thin-films.[113] The substrates were unidirectionally abraded with nanodiamond ultra lapping film to create nanogrooved texture, Fig. 16(d). Surface and bulk characterization of the solution sheared films of poly[4-(4,4- dihexadecyl-4H-cyclopenta[1,2-b:5,4-b′]dithiophen-2-yl)-alt-[1,2,5] thiadiazolo[3,4-c]pyridine] (PCDTPT) and CDTBTZ exhibited that CPs at the bottom possessed high orientation along the length of the nanogrooves. However molecular orientation along the film thickness changed as a function of coating speed and direction and the same was reflected in their charge transport property as shown in Fig. 16 (e).

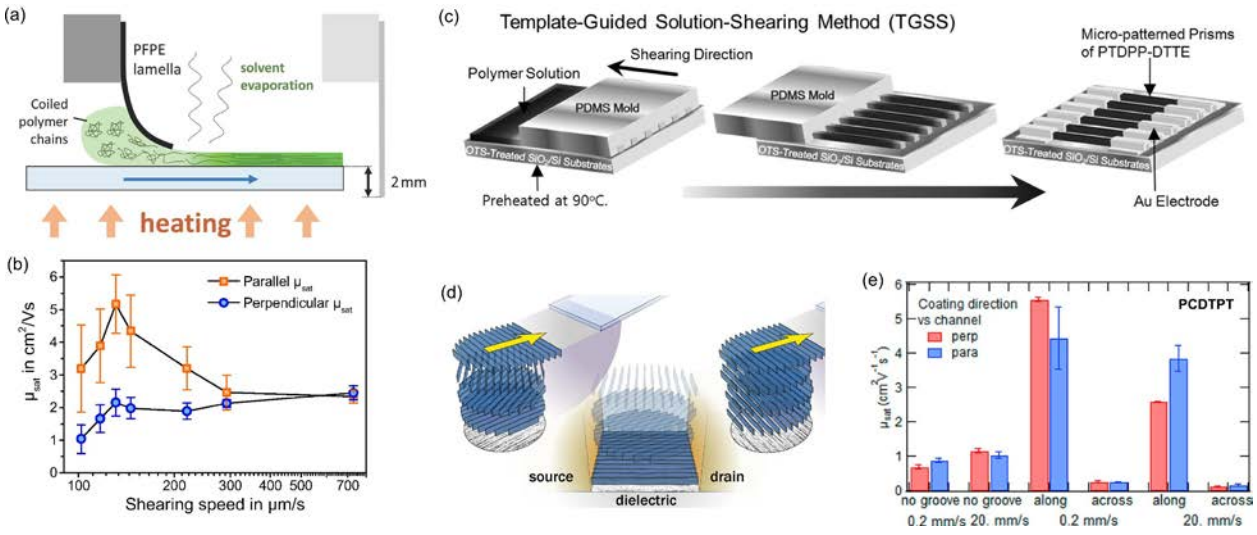

Fig. 16. (a) Schematic representation of shearing setup, where the sample is fixed on top of a heated stage. (b) Shearing speed dependent variation in hole mobilities of FETs with aligned polymeric (DPP-BTz) layers, parallel and perpendicular to shearing direction. (Reprinted with permission from 79.) (c) Template-guided solution-shearing (TGSS) method using a PDMS mold with uniaxially aligned microgrooves. (Reprinted with permission from 112. Copyright 2014, John Wiley & Sons.) (d) The schematic representation for solution-shearing on nanostructured (nano-grooved) substrate. (e) Hole mobilities in the polymer (PCDTPT) thin films casted in different conditions. The parallel and perpendicular corresponds to the coating direction relative to the channel. Along and across is defined as the coating direction with respect to the nanogrooves, if both are aligned termed as 'along' and for the orthogonal case it is 'across', which are left and right sides of (d)-part respectively. (Reprinted with permission from 113. Copyright 2018, American Chemical Society.)

Extensive work has been done by Xu et al. towards the application of solution-shearing technique for the preparation of meter-scale roll-to-roll flexible and stretchable CP thin films.[115] Through a microtrench-pattered coating blade, macroscopic orientation of CP's nanostructures was achieved leading to the subsequent reduction in the energy barrier for charge transport by the short-range π–π ordering due to nanoconfinement effect, **Fig. 17.** The field-effect mobilities of stretchable films of five different CPs processed through this technique have been enhanced by 6-fold compared to the spin-coated films and the mobility was almost unchanged under a strain up to 100% (Fig. 17 (c)). Such an extensive research work carried out in solution sheering depicts that

there exist a great possibility towards the facile fabrication of oriented polymer thin films and their application in high performance printed electronics. However, in some cases, the molecular structure-dependent performance limits its application to a specific set of CPs. At the same time, it seems difficult to fabricate organic devices with multi-layered organic thin films utilizing different CPs.

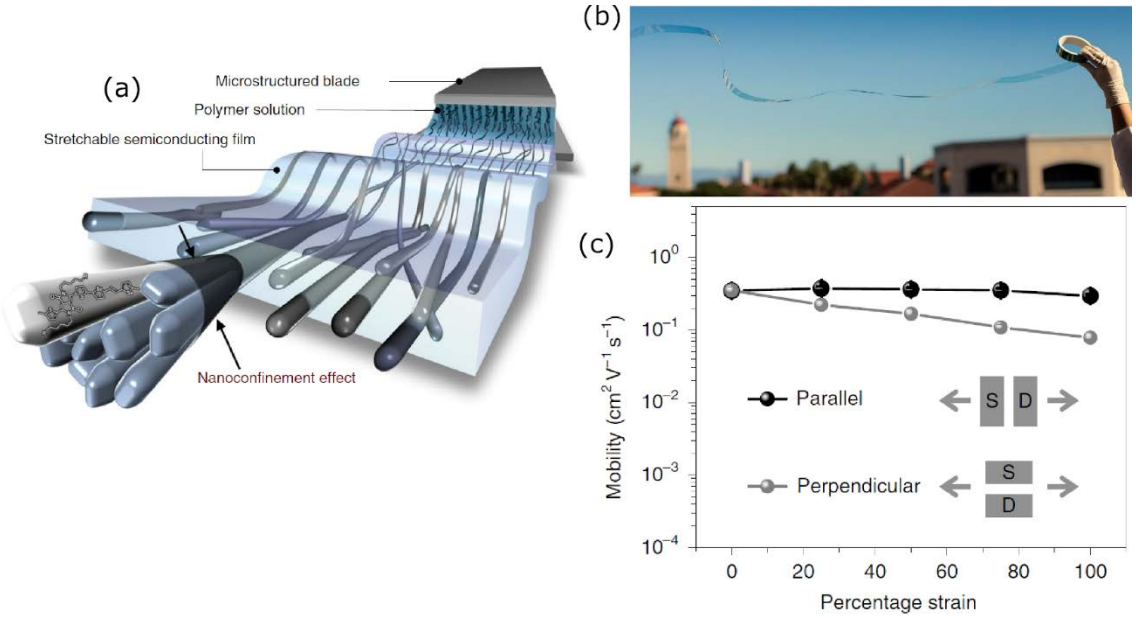

Fig. 17. (a) Three-dimensional schematic representing alignment of polymer nanofibers through the solution-shearing method using a microtrench-patterned blade. (b) Roll of meter-scale, roll-to-roll-coated CONPHINE films on PET. (c) Changes in the mobility (calculated with measured device geometry and dielectric capacitance under strain[116] of the roll-to-roll-coated CONPHINE film with strain up to 100%, both parallel and perpendicular to the charge transport direction in the fabricated fully stretchable transistors. CONPHINE: conjugated-polymer/elastomer phase-separation-induced elasticity. (Reprinted with permission from 115. Copyright 2019, Springer Nature.)

3.1.4 Wire Bar Coating: This meniscus guided coating technique consists of a cylindrical bar wounded with wire of specific diameter and a mobile stage to mount the substrate, which can move against the coating bar, as shown in the **Fig. 18**. Wire-bar is kept close to the substrate and polymer solution is placed before it such that solution meniscus can adhere to it. Due to relative

motion between substrate and the wire-bar, excess solution is wiped out leaving the polymer thin film on the substrate. Effective separation between them controls the rate of solution flow deciding the film thickness. However solution rheology, viscosity and concentration are also crucial parameters controlling the film morphology.[75,117,118] Initially Ouyang et al. demonstrated fabrication of large area polymer based organic light emitting diodes utilizing thin films of the light emitting polymer MEH-PPV using continuous bar coating[119]. However, fabrication of polymer based OFETs was first reported by Murphy et al, where they fabricated thin film of P3HT and insulating high-density polyethylene blend by this technique and reported charge carrier mobility reaching up to 0.05 $cm^2/V.s$.[120] Future scope of this technique in the roll-to-roll fabrication of printed electronics can be gauged by the extensive reports from the Noh's group, in which they demonstrated dens array of OFETs with high yield and low device to device variations[121,122].

For the first time application of this technique for anisotropic film fabrication was reported by Bucella et al., where they emphasized the importance of the pre-aggregation in solution ink for the film anisotropy, Fig. 18.[77] They fabricated thin film of P(NDI2OD-T2) dissolved in mesitylene (a poor solvent) with backbone oriented along the coting direction. The oriented film exhibited average mobility of 4.1 ± 1.4 $cm^2/V.s.$ with the $\mu_{\parallel}/\mu_{\perp} > 10$), which was higher that obtained for isotropic spin-coated films (1.06 ± 0.69 $cm^2/V.s$). In the same report, they also demonstrated the effect of molecular weight on charge transport using wire-bar coated thin films of varying molecular weight P(NDIOD-T2). The thin films fabricated with moderate M_w CP (20–26 kDa) were found to be better for the facile charge transport, which was attributed balanced orientation with less inter-chain entanglement. Recently Jiang et al. investigated the role of coating speed and substrate temperature on the wire-bar coated film morphology, however, preaggrigation in solution

was essentially followed. They reported that orientation increased with the increasing coating speed, Fig. 18 (c – f).[80] Moreover, low casting temperature (60 °C) was found to be optimum, by keeping the balanced solvent evaporation rate and pre-aggregation in the solution. Consequently in the optimum condition, the wire-bar coated thin films of poly(fluoroisoindigodifluorobithiophene-fluoroisoindigo-bithiophene) (PFIBI-BT), exhibited almost ninefold enhancement in the hole and electron mobilities ($\mu_{\parallel,h}$ = 5.1 cm^2/V.s and $\mu_{\parallel,e}$ = 4.2 cm^2/V.s with $\mu_{\parallel}/\mu_{\perp}$>3), as compared to the corresponding spin coated ones (μ_h = 0.6 cm^2/V.s and μ_e = 0.4 cm^2/V.s) .

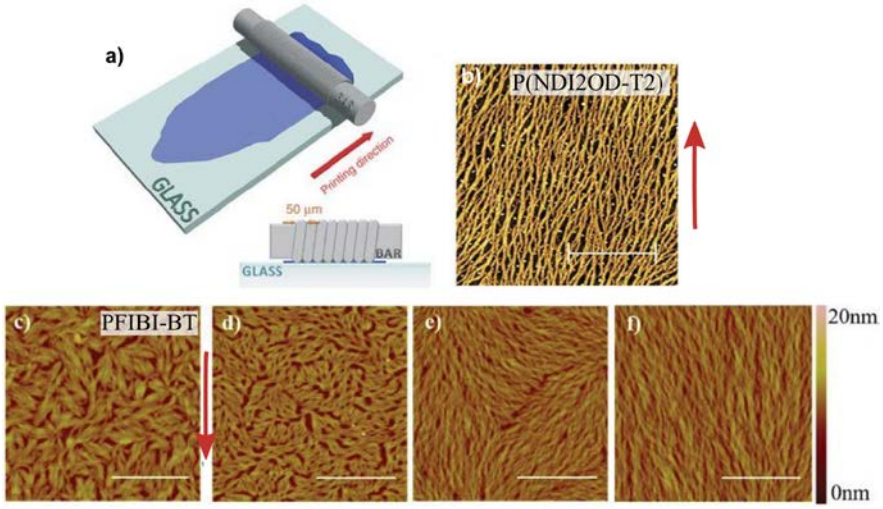

Fig. 18. (a) Schematic illustration of the wire-bar coating technique. (b) AFM picture of a P(NDI2OD-T2) thin film deposited by bar-coating from a 0.5 g/l solution in mesitylene. Scale bar is 1 µm. (Reprinted from 77.) AFM images of PFIBI-BT films prepared by (c) spin-coating and (d – f) bar coating at varying coating speeds of (d) 40 mm/s, (e) 80 mm/s, and (f) 120 mm/s. Scale bar is 2 µm. (Reprinted with permission from 80. Copyright 2019, John Wiley & Sons.)

Although this method provides uniform thin films but here are chances of the mechanical damage since the wire is in direct contact with the film and very close to the substrate. For instance, if the underlying layer is a soft material, then it may get scratched or the dielectric interface may get distorted.

3.2 Off-Center Spin Coating

The off-center spin coating (OCSC) method was primarily introduced by Bao group, where they reported highly aligned semiconducting organic molecule 2,7-oxtyl[1]benzothieno[3,2-b][1]benzothiophene (C8-BTBT) blended with polystyrene (PS).[123] In this method, the substrate is placed away from the spin center and under high rotational speed, huge centrifugal force acts on the solution as shown schematically in the **Fig. 19**. Due to the combined effects of centrifugal force, solution viscosity and substrate-solution interfacial interactions, macromolecules get aligned. However, the effect of outward drag on top layer of the solution remains maximum and decreases with the depth, resulting in to highly oriented top layer. They reported radial alignment of the C8-BTBT/PS matrix, where resultant field-effect mobility reached up to 43 $cm^2/V.s$ in the aligned C8-BTBT/PS matrix. Later, Applicability of this method to orient CPs was reported by Wang et al. with an in-depth investigation of various controlling factors responsible for the orientation.[124] However, Matsidik et al. first utilized this technique to fabricate CP based OFETs.[125] They demonstrated the improved field-effect mobility in off-center spin coated P(NDI2OD-T2) with an average value of 2.6 $cm^2/V.s$, which was much higher in comparison to the devices for conventional spin coating lying in the range of 0.1 – 0.6 $cm^2V^{-1}s^{-1}$.[126]

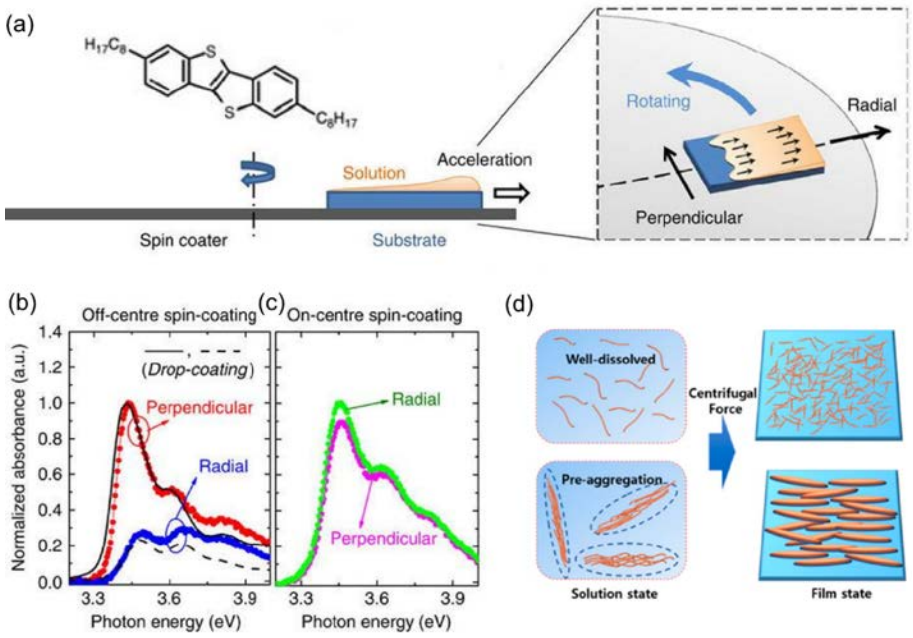

Fig 19. (a) Chemical structure of C8-BTBT with schematic illustration of the OCSC process, in which the substrates are located away from the axis of the spin-coater. (b) Normalized polarized-absorption spectrum of OCSC C8-BTBT:PS film, where the light electrical field is in radial (blue circles) or perpendicular direction (red circles) and the directions are marked in the Fig. 19 (a), (**c**) Normalized polarized-absorption spectrum of on-center spin-coated C8-BTBT:PS film, where the light electrical field is in radial (green circles) or perpendicular direction (pink circles). (Reprinted with permission from 123. Copyright 2014, Springer Nature). (d) Schematic illustration of well-dissolved and pre-aggregated polymer in solution state and solid state. (Reprinted with permission from 127. Copyright 2015, American Chemical Society.)

Later, comprehensive study on wide range of CPs was reported by Noh group, where they validated the inevitability of pre-aggregation in solution for macromolecular orientation.[127] For instance P(NDI2OD-T2) dissolved in both good (chlorobenzene, CB) and poor (toluene, Tol) solvents to fabricate thin films and investigate the implications of pre-aggregation assisted molecular self-assembly on the device performance. It was observed that utilization of relatively poor solvent during thin film fabrication not only exhibited improved field-effect mobility but also the higher and higher electrical anisotropy [$\mu_{\parallel} \approx 0.6$ cm^2/V.s (CB) and 1 cm^2/V.s (Tol); $\mu_{\parallel}/\mu_{\perp} \approx 5$ (CB) and 9 (Tol)]. Through the surface characterization, it was also evidenced that orientation occurs primarily at lop layers of the film resulting in the negligible changes in the DR of the bulk,

however, high $\mu_{\parallel}/\mu_{\perp}$ was obtained for top-gated bottom-contact OFETs. In the following work, they demonstrated the solvent optimization approaches to improve carrier transport in the off-centered spin-coated thin films.[128,129] They reported that similar molecular interaction between solvent and CP (by analyzing Hansen solubility parameters) results in a larger and ordered domain in thin films.[130] By analyzing various solvent system, high boiling point solvents with poor solubility of the CP were found suitable to orient thin films by OCSC technique.

Improvisation in the OCSC method has also been attempted by optimizing the forces involved in the spin coating. Noh group reported a *rotation coating technique*, which can considered as a modified version of standard OCSC technique as schematically shown in **Fig. 20**[131]. In this modification, spinning axis was made to lie in horizontal direction by tilting the spin coater unit, where substrate plane was perpendicular to the spinning axis. Aim of this modification was to utilize the centrifugal force to allow the solution to remain with the substrate and inertial force to induce orientation in the polymer chains. This method also facilitated high orientation in Poly[2,5-(2-octyldodecyl)-3,6-diketopyrrolopyrrole-alt-5,5-(2,5-di(thien-2-yl)thieno [3,2-b]thiophene)] (DPPT-TT) with DR of ~3, which was higher than that observed for the conventional off-center spin-coating technique reported by the same group earlier. Huang et al. have used inverted off-center spin-coating technique, which was consisted of two steps, at first the solution is spun by standard off-center spin coating followed by putting the substrate upside-down.[132] In this, combined effect of centrifugal force and gravitation force as well as presence of high boiling point solvent additive led to the improved vertical donor-acceptor gradient in organic solar cells. Although OCSC technique is easy to implement for demonstrating high charge transport property at laboratory-scale, drawbacks such as the amount of material wastage and limited substrate size withhold it from large area applications for the future printable electronic devices. However, the

later modifications made by Noh group and Huang et al. offers unique advantages over the conventional OCSC method.

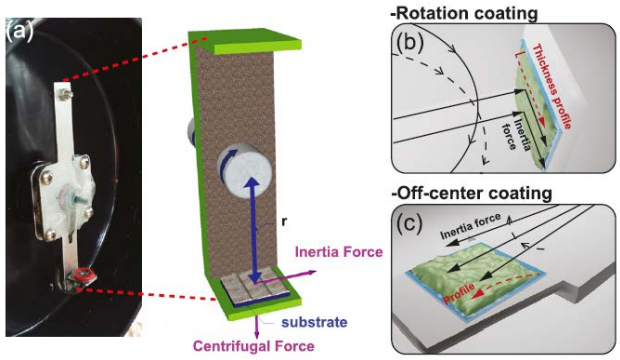

Fig. 20. (a) Digital camera image and schematic illustration of the proposed rotation coating system, with a model of the inertial direction and centrifugal force acting on polymer solution. (b) Schematic illustration of inertial force direction and thickness profiles in rotation coating and (c) off-center spin coating method. (Reprinted from Ref. 131, with the permission of AIP Publishing.)

3.3 Floating Film Transfer Method

Floating film transfer method (FTM) was developed by our group aiming towards the fabrication of thin floating films of CPs on an orthogonal liquid substrate followed by the transfer of solid floating films on any desired substrate by simple stamping. Although FTM looks similar to Langmuir-Schaefer technique; however controlling the surface pressure to make a compact film is not required.[133] In our early report, we demonstrated the fabrication of thin floating films of Regioregular P3HT (RR-P3HT), where transport characteristics were enhanced by an order of magnitude in comparison to spin-coated devices due to high film crystallinity. Though macroscopic orientation in RR-P3HT was not observed, well-ordered P3HT domains with well-stretched polymer chains standing on the substrate having π-π stacking in plane of the substrate (edge-on dominated orientation) were clearly demonstrated. Even though film fabrication process was carried out under ambient laboratory condition, low film conductivity (off current) was

conserved reflecting absence of any contamination arising from the components of liquid substrate during the film fabrication. Thin film fabrication by this method involves three steps: 1) casting a drop of the polymer solution in the center of the petri-dish containing hydrophilic liquid substrate, 2) allowing the polymer solution to spread followed by solvent evaporation and 3) transferring the floating film on any desired substrate by stamping; which has been schematically shown in **Fig. 21**.

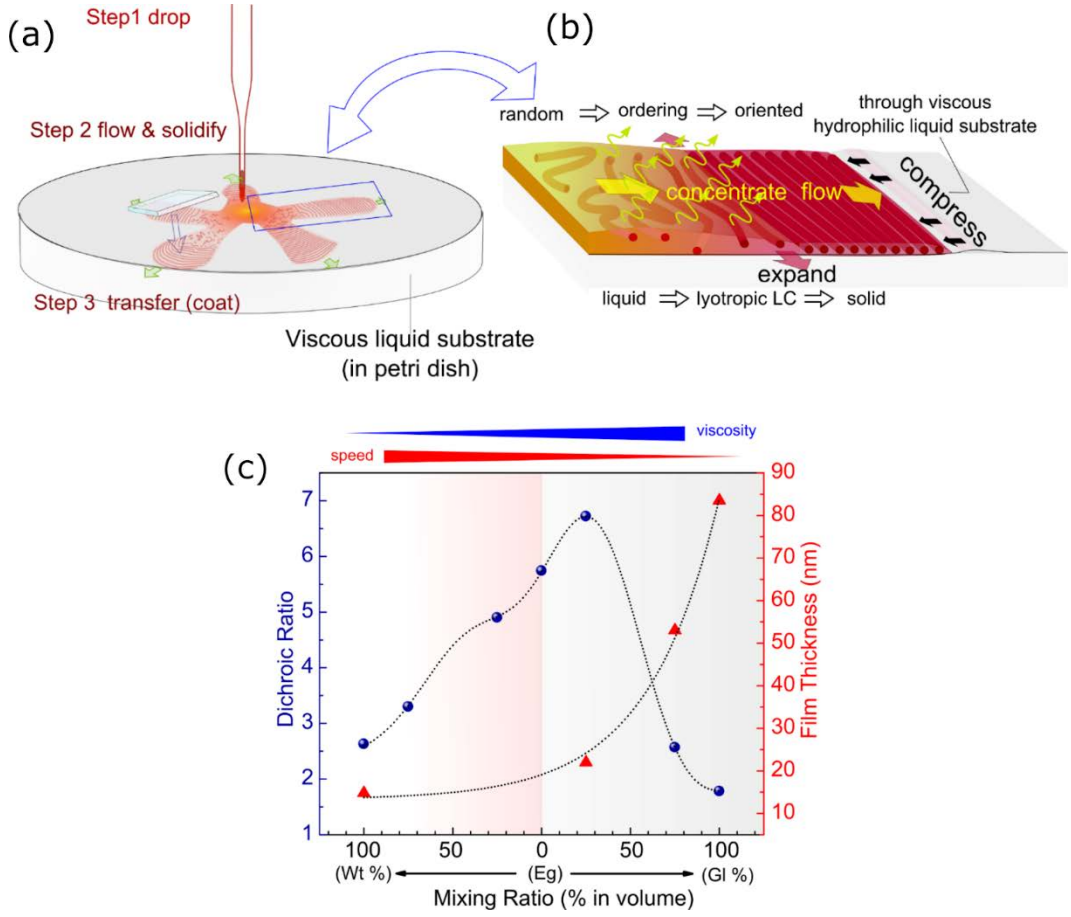

Fig. 21. Schematic illustration of floating film transfer method (a) and associated possible mechanism for orientation in FTM (b). DR variation in FTM film of NR-P3HT with different liquid as a function of mixing ratio in various binary liquid-substrates Wt, Eg and Gl.

Later, this method was extensively used by us and many different research group for the orientation of many well-known CPs for organic electronic devices, such PFO, (9,9-

dioctylfluorene-co-benzothiadiazole) (F8BT), poly9,9-dioctyl-fluorene-co-bithiophene (F8T2), PQT, PBTTT, Non-regiocontrolled P3HT (NR-P3HT), RR-P3HT, *defect-free* P3HT, diketopyrrolopyrrole-naphthalene, diketopyrrolopyrrole-naphthalene (PDPP-TNT), poly(bis(5-(dodecyloxy)-2-nitrobenzyl) 1-(5-(2,5-difluoro-4-(thiophen-2-yl)phenyl)-thiophen-2-yl)-4H-cyclopenta[c]thiophene-5,5(6H)-dicarboxylate) (CP1-P).[134–145] The isolation between the film casting and transfer gives enough freedom to control the desired morphology of quasi 1-dimensional CPs. It was found that judicious control of parameters of casting during the film fabrication can induce macroscopic orientation of CPs. Therefore, it was found that proper control of the casting condition, such as viscosity and temperature of the liquid substrate, concentration and mixture component of the polymer solution induce very high orientation.

In this method, the viscosity of the hydrophilic liquid substrate provides the compressive force which hinders spreading of the floating film and control the speed of the film formation at the same time. The viscosity of liquid substrate and its temperatures should be optimized depending on the nature of CP under investigation.[140,142,144,146,147] Standard viscosity of the three different liquid substrates distilled water (Wt), ethylene glycol (Eg), and glycerol (Gl), at 30°C are 0.79, 14.41 and 487.64 centistokes, respectively.[148–150] Mixture of any two of these hydrophilic liquid substrates are often used to tune the viscosity values. Although viscosity values of resulting mixtures are generally not reported since mixtures are prepared to optimize DR. However, viscosity of mixtures can be calculated precisely by lengthy experimental procedure or through calculations using the double-logarithmic equation of Refutas.[140,151] Variation of DR and floating film thickness of NR-P3HT with varying liquid substrate combinations are shown in **Fig. 21**, which clearly reflects the advantages of tuning the viscosity for controlling the oriented film with desired DR and thickness.[147] Similarly, the effect of changing the NR-P3HT concentration and

temperature of liquid substrate critically affects the DR as already reported by our group and needs to be optimized in order to get highly oriented film.[140,141]

Qualitative analysis of orientation and implication of such a high DR in NR-P3HT was well reflected by the drastic improvement in film crystallinity and charge transport behavior as shown in **Fig. 22**.[137,141] Out-of-plane XRD of FTM coated NR-P3HT showed intense (*a00*) diffraction peak related to lamellar alkyl-stacking representing edge-on orientation whereas only (*020*) diffraction peak related to π-π stacking was observed for spin-coated NR-P3HT films reflecting the face-on orientation (Fig. 22 (a)). Uniaxial orientation of NR-P3HT in FTM films were also confirmed through in-plane GIXD reflecting the presence of π-π stacking peak in-plane of the substrate (Fig. 22 (b)). NR-P3HT possesses low regioregularity of ~ 80% and their spin-coated films are known to have amorphous morphology resulting into their low OEFT mobility in the order ~10^{-5} $cm^2V^{-1}s^{-1}$. We reported that FTM coated NR-P3HT results in remarkable enhancement of OFET mobility by ~2 orders in magnitude with $\mu_{\parallel}/\mu_{\perp}$ ~ 5 with the maximum mobility reaching up to 3.4×10^{-5} $cm^2V^{-1}s^{-1}$ due to the formation of oriented fibrous domains, which were absent in the spin-coated films.[141]

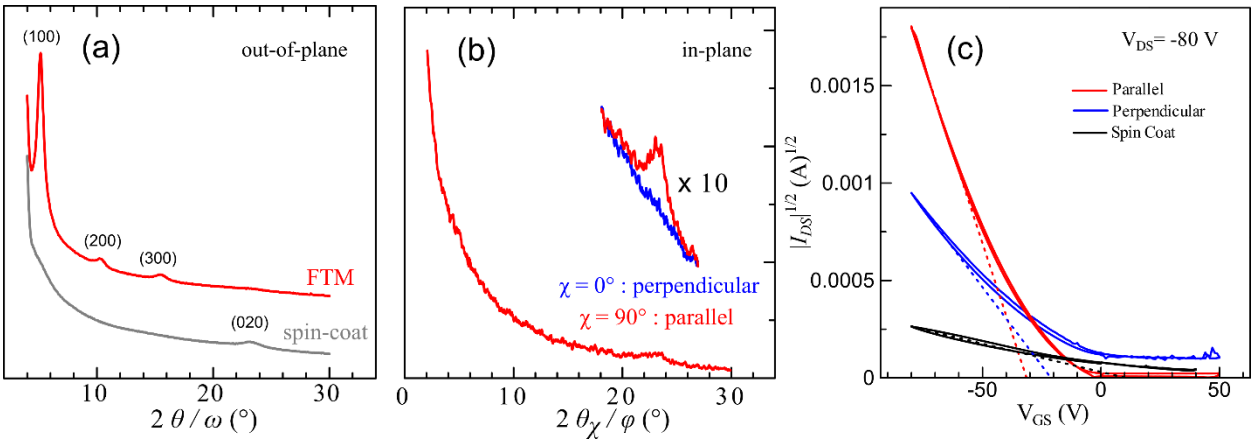

Fig. 22. (a) Out-of-plane XRD pattern of FTM and spin-coated film of NR-P3HT. (b) In-plane GIXD of NR-P3HT film prepared by FTM. Permission request to reuse this figure is in process with publisher. (c) Transfer curves of NR-P3HT prepared with different channel configurations. (Reprinted with permission from 141. Copyright 2016, Elsevier.)

Recently, using FTM and same casting procedure condition, Nawaz et al. have demonstrated excellent field-effect mobility of 8 $cm^2V^{-1}s^{-1}$ in *defect-free* P3HT (100% regioregular).[143,145] The same group has also reported improvement in mobility up to 1.3 $cm^2V^{-1}s^{-1}$ for co-polymer PDPP-TNT.[143,145] They used cross-linked poly(vinyl alcohol) as the gate insulator for low voltage operation of OFET, and in the case of spin-coating of PDPP-TNT, the transistor property was highly deteriorated due to the interaction between CP and dielectric at the interface. Since the active channel layers in FTM are transferred in the *dried state* on the substrate; therefore, the absence of solvent interaction would always be the reason for achieving superior OFET performance. Film preparation using solvent often deteriorate the organic gate dielectrics even if solvent orthogonality would be considered. Due to 2-order magnitude enhancement in NR-P3HT, we have also reported the possibility of further enhancement in their orientation by blending it with highly crystalline PBTTT that resulted in to synergistic enhancement of OFET mobility and orientation of the NR-P3HT. The enhancement in the blend was due to the decrease in entanglement of NR-P3HT domains arising from the addition of crystalline guest PBTTT.[152]

We have further demonstrated the fabrication of *layer-by-layer* coating of oriented films preserving the complete morphology of the underlying layers as shown in **Fig. 23**. Since thickness and DR cannot be optimized at the same time in FTM; therefore, this method can be used to obtain any desired film thickness. UV-vis polarized absorption and DR of *layer-by-layer* of NR-P3HT film (each layer oriented parallel to each other) and PQT/F8T2 with orthogonal orientation is shown in Fig. 23. These results demonstrate that the DR can be well preserved in the underlying layers and number of layers can be increased in order to obtain desired thickness. At the same time, orthogonally coated oriented films of PQT and F8T2 with different absorption is shown in Fig. 23

(d) indicate the retention of their respective vibronic features. Although importance of such orthogonally coated oriented film in device application is still needs to be realized; however, bandgap difference between the individual layers allows the possibility of wavelength selective polarized emission as schematically illustrated in Fig. 23 (f). Strong vibronic modes retained by both PQT and F8T2 layer indicates their extended π-conjugation length and absence of any possible interference arising in the film-morphologies of both the under- as well as the over-layers even after orthogonal coating.

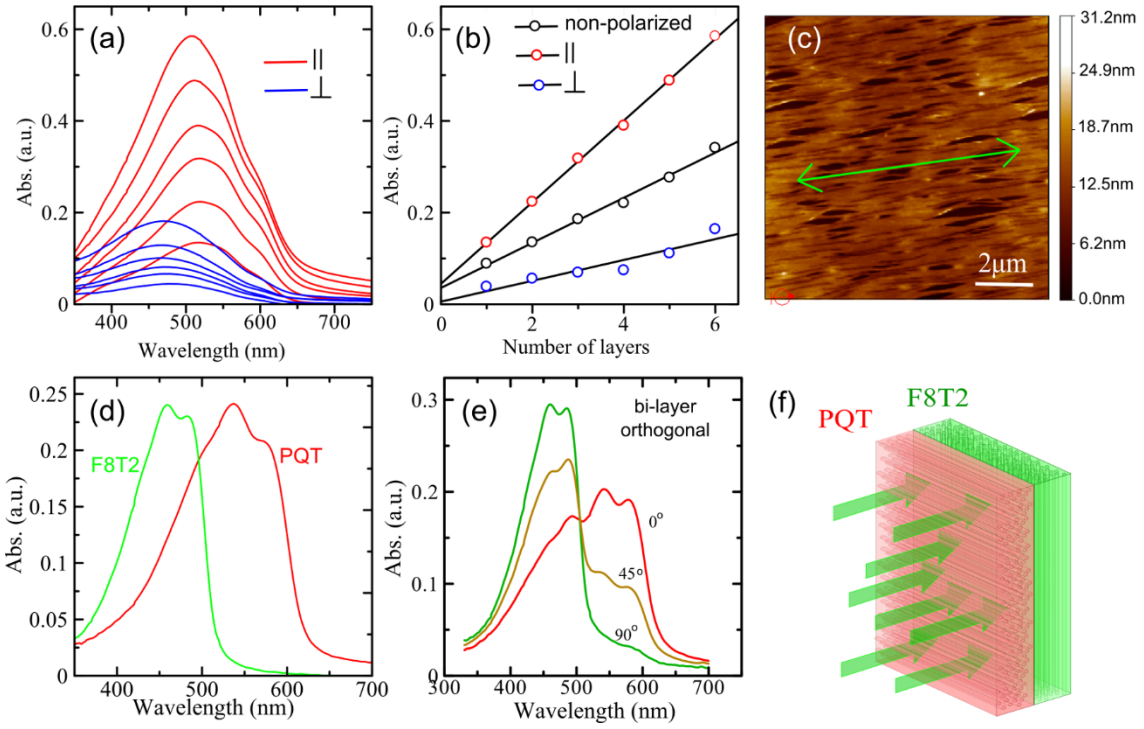

Fig. 23. Evolution of polarized absorption spectra with multi-layer coated NR-P3HT (a), peak height of the corresponding polarized absorption with increase in number of layers (b) and AFM image of the oriented NR-P3HT by FTM (c). Absorption spectra of spin-coated (d) and orthogonally coated F8T2 and PQT by FTM (e). (f) Schematic illustration of the polarized monochromatic (about 480 nm) light illumination parallel to F8T2 orientation. Permission request to reuse this figure is in process with publisher.

FTM method was later applied to highly promising rigid rod-like high-performance liquid crystalline CP, PBTTT and DR of the as-cast FTM films were found to be in the range of 3.2~4

reaching up to 6.[142,146] However, there was remarkable improvements in the DR (10-13) of PBTTT films observed when annealed at their ribbon-phase temperature where polymer side chain melts and initial alignment serve as a template to assist macromolecules to align uniaxially.[142,153,154] The GIXD results of PBTTT coated by FTM and spin coating method showed that PBTTT tends to orient in edge-on conformation; however, FTM films possess high crystallinity than that of many of the other coating methods. Though PBTTT is known to take edge-on conformation in the films prepared with most of the conventional coating techniques excluding those where shear forces change the configuration from edge-on to face-on while orienting them.[58] However, in case of as-prepared FTM films, out-of-plane diffraction (*h00*) peaks appeared at lower angle making this stacking distance larger to that of spin-coated films. This was supposed to occur due to high repulsion between the hydrophilic liquid substrate and long alkyl side chains of the PBTTT which later decreases to the same distance as of spin-coated one through recrystallization after post-annealing as can be seen in **Fig. 24** (a, b). The complete absence of (*h00*) and appearance of π-π stacking peak in in-plane GIXD pattern revealed that main chains were ideally oriented with the absence of any face-on oriented crystallites. The average field-effect mobility of along the orientation direction reached up to 1.24 $cm^2V^{-1}s^{-1}$ and was higher by an order of magnitude than the spin-coated reference sample. The angle-dependent mobility measurement clearly reflected a drop in mobility by 6-fold when channel direction was at 30˚ with respect to the orientation direction. This clearly state the need and advantages of such a high orientation since charge transport in CPs is dominated through intrachain assisted by tie-chains and π-π stacking as illustrated in Fig. 24 (e).

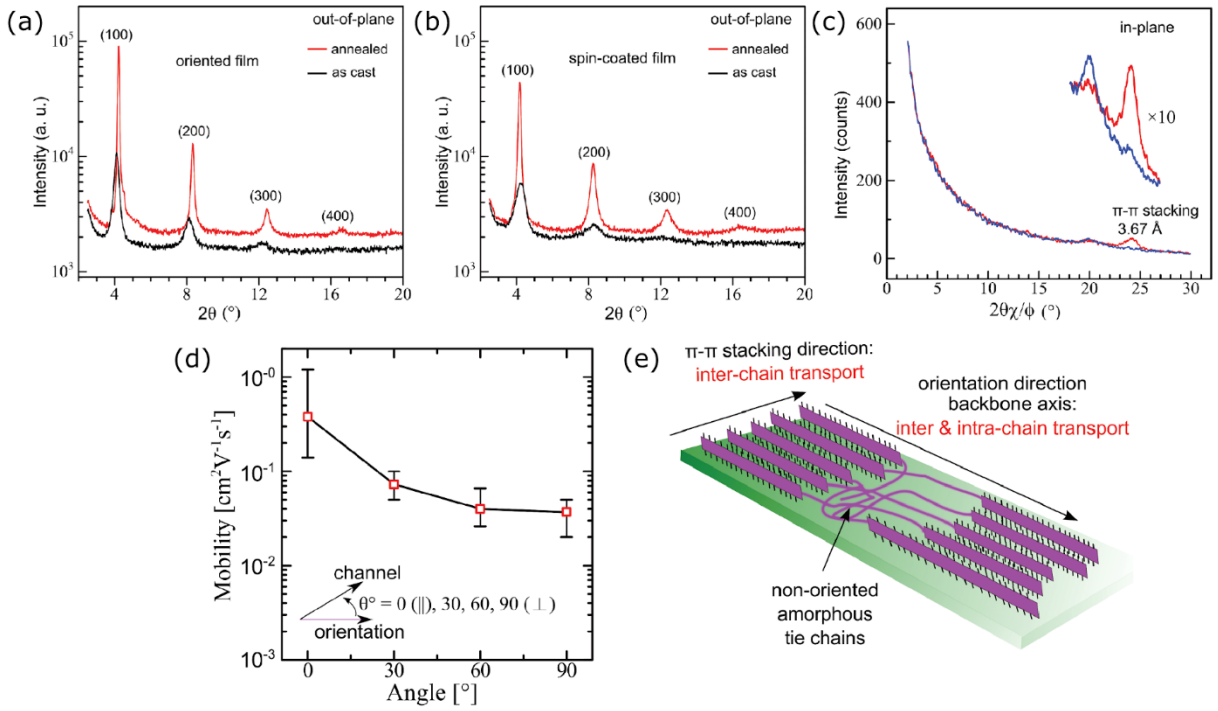

Fig. 24. Out-of-plane XRD pattern of FTM and spin-coated films of PBTTT (a and b). In-plane GIXD pattern of oriented FTM film of PBTTT (c). Variation of the field-effect mobility at different angles with respect to the orientation direction (d). Schematic illustration showing the possible charge transport pathway in edge-on oriented crystallites (e). (Reprinted with permission from 142. Copyright 2018, John Wiley & Sons.)

Characteristics differences in FTM film of CPs with low and high boiling point (BP) solvent was demonstrated by our group and it was found that low BP solvent i.e. chloroform should be preferred over other solvents with high BP i.e. chlorobenzene. Solvents with low BP like chloroforms tends to evaporate very fast while spreading the polymer solution and local ordering of them must be governed by lyotropic LC behavior of CPs. Our investigation revealed that CPs with inherent LC behaviour exhibit high molecular orientation in FTM films; therefore, their orientation must be getting governed by lyotropic phase-assisted self-assembly during rapid solvent evaporation and dragging forces acting in direction opposite to the film spreading due to viscosity of the liquid substrate.[144] Although the use of high BP solvent induces self-assembly and helps in forming large crystalline domains in CPs, complete replacement of low BP solvent with

high BP solvent impact the macroscopic chain alignment in FTM according to a recent report by Yang et al., where they demonstrated a new solvent composition in FTM.[146,155,156] Therefore, they precisely controlled the solvent composition using high BP solvent as an additive to allow adequate time for polymer chains to self-assemble.[134] They found that high DR and field effect mobility in CP1-P when high BP solvent 1, 2 dichorobenzene (DCB) was utilized as an additive to chloroform in the FTM process. As shown **Fig. 25**, They obtained DR of 4.8 with the use of solvent blend of DCB and chloroform (in the ratio 3: 97) in comparison to DR of < 1.5 with chloroform and any further addition of DCB significantly decreases the DR of the CP1-P films.

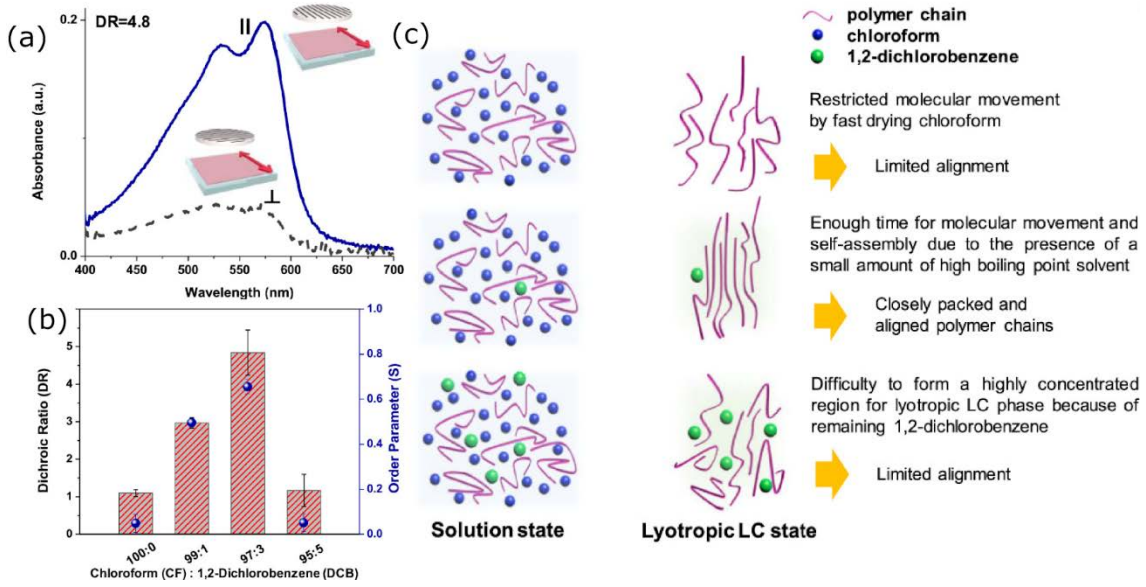

Fig. 25. (a) Polarized UV–vis absorption spectra of the CP1-P film from the solution in CF with 3 vol % DCB. The inset represents the directions of linear polarizer (black lines) and polymer chain alignment (red arrow), respectively. (b) DR (the bar graph) and order parameter (*S*, the blue solid sphere) as a function of CF-DCB blend ratios. The error bars represent the standard deviation. All films were formed by FTM on the subphase liquid of ethylene glycol–glycerol blend (1:1 v/v). (c) Schematic illustration of the FTM film formation mechanism by CP1-P solution in CF and CF/DCB (97:3 v/v), respectively. (Reprinted with permission from 134. Copyright 2018, American Chemical Society.)

It is important to consider that although this method of casting FTM films in petri-dish filled with liquid substrate seems easy and highly cost-effective approach; However, obvious differences in quality of films arising from hand to hand and sample to sample variation is a key issue. To circumvent this problem, our group has recently reported a modified form of FTM technique known as ribbon-shaped FTM as schematically illustrated in **Fig. 26** (a).[157] Where a custom made slider was placed in a rectangular tray containing liquid substrate, such that the inclined bottom surface of the slider partially immerse inside the liquid. In this condition, when the polymer ink of (15-20 µl) is placed at the junction of slider's bottom surface and liquid substrate, the slope of the slider allows film growth in forward direction and the presence of side walls prevents the spreading films in other direction which results in large area ribbon-like anisotropic FTM film. Further, We have also demonstrated the versatility of this ribbon-shaped FTM film to prepare large area (> 2 cm × 15 cm) oriented thin films along with the investigation of anisotropic charge transport.[158]

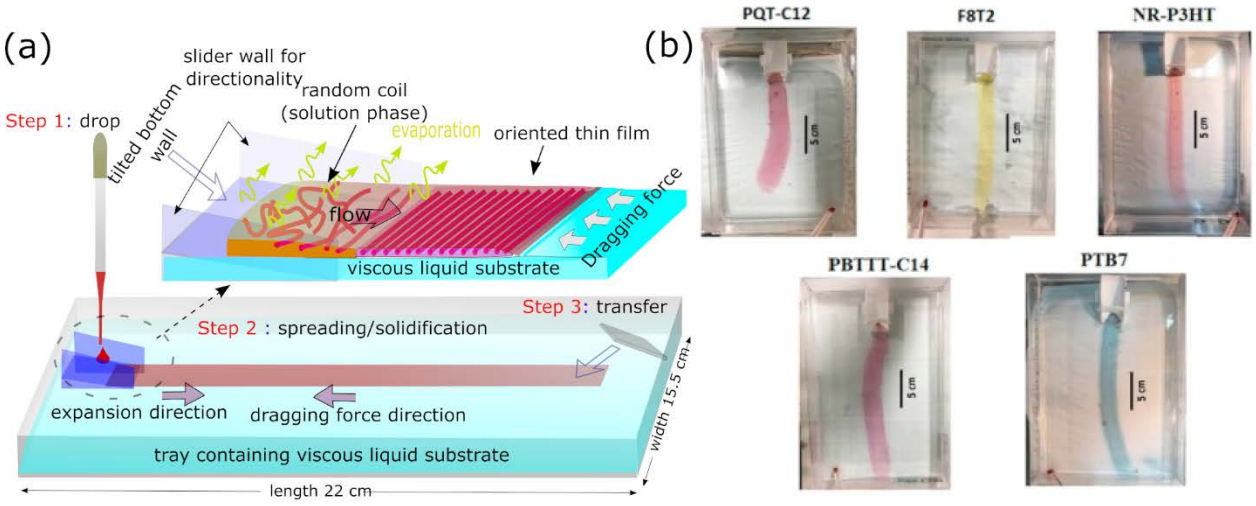

Fig. 26. (a) Schematic representation of fabrication of ribbon-shaped FTM film. (Reprinted from 157 with the permission of AIP Publishing.) (b) Photograph of the large thin films of various CPs prepared in a rectangular tray of 15 cm x 25 cm. (Reprinted with permission from 158. Copyright 2019, Elsevier.)

Although this method is able to provide large area oriented thin film of CPs at low cost which qualifies it for application in the mass fabrication of organic electronic devices, the fabrication of small molecular semiconductor thin film is an arduous job. At the same time, application of this method is only limited to CPs having good solubility in low BP solvent.

3.4 Directional Solvent Evaporation on Nanostructured Substrate

Consistent and thorough studies on orientation of CPs through directional solvent evaporation on nanogrooved substrates and its application for high performance OFETs have been reported by Herger group.[159–163] In this technique, two SiO_2 substrates abraded with diamond lapping films were placed face-to-face separated by two glass spacers making a tunnel-like configuration, which confined the direction of the solvent evaporation as shown in **Fig. 27** (a and b). Moreover, by keeping the system in a covered petri dish, the rate of solvent evaporation was further slowed down leading to long-range alignment of polymer nanofibers, Fig. 27 (c and d). Orientation in a high M_w (300 kDa) donor-acceptor type copolymer PCDTPT led to hole mobility of 6.7 $cm^2/V.s$ (with $\mu_{\parallel}/\mu_{\perp} \approx 6$).[159] Efforts were directed to enhance the field effect mobility further by tuning the molecular weight,[160] impurity doping[161] and surface modification of dielectric layer.[162] Eventually significantly high mobility of 56.1 $cm^2V^{-1}s^{-1}$ was demonstrated for iodine vapor treated directionally aligned PCDTPT thin films.[161] Fabrication of high performance flexible OFETs with hole mobility reaching of 10.5 $cm^2/V.s$ was also demonstrated by the same group.[163]

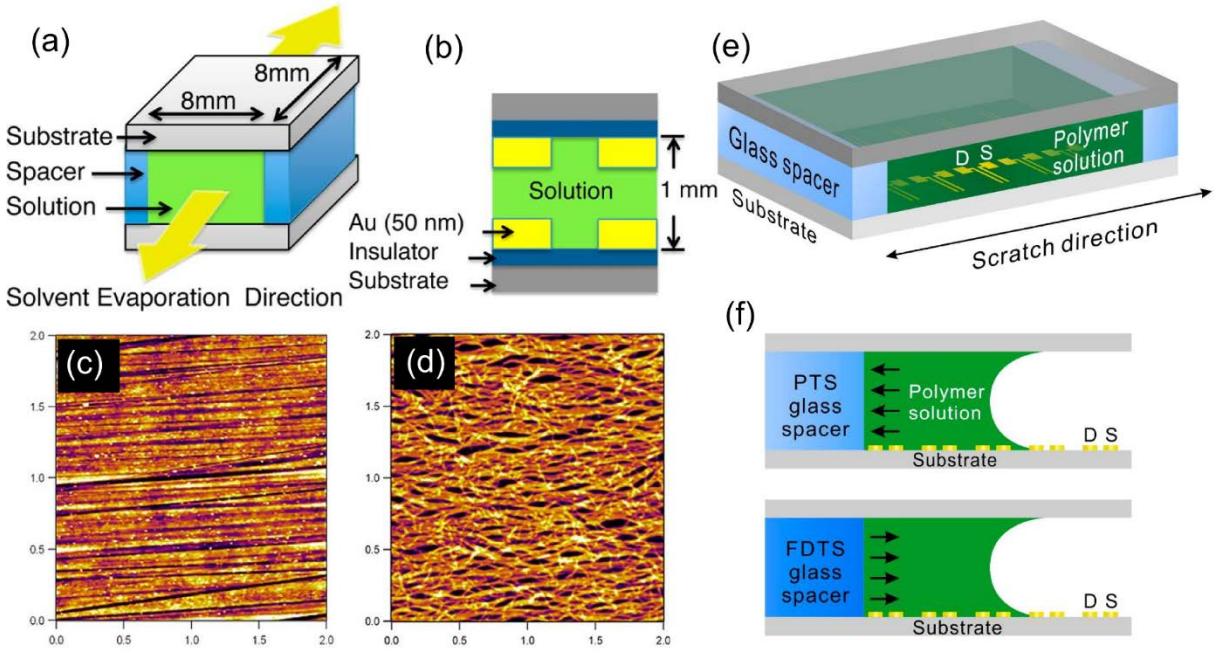

Fig. 27. (a) Cartoon illustration of the tunnel-like configuration setup and (b) Cross-sectional illustration for directional solvent drying. The pictures are not to scale. AFM images of (c) dielectric substrate surface scratched by diamond lapping films with nanoparticle diameters of 100 nm and (d) corresponding PCDTPT layers coated on it through directional solvent evaporation technique. (Reprinted with permission from 159. Copyright 2012, American Chemical Society.) (e) Schematic illustration of the sandwich tunnel system consisting of two silicon substrates (12.2 × 7.7 × 0.5 mm) with a pair of glass spacers (7.7 × 2.0 × 1.0 mm) inserted at two ends. Polymer solution (75 μL) was added into the tunnel (8.2 × 7.7 × 1.0 mm). D and S denote the bottom-contact drain and source electrode, respectively. (f) Schematic diagram (side view) showing the different actions to the polymer solution exerted by the spacers with two opposite surface treatments, PTS (top) and FDTS (bottom), respectively. (Reprinted with permission from 164. Copyright 2014, American Chemical Society.)

To improve the polymeric self-assembly, the combined effect of capillary action due to glass spacers and gravitational drag due to substrate inclination were also optimized.[164] The effect of capillary action was optimized by tuning the surface energy of the spacers and for that they were subjected to functionalization with different self-assembled monolayers such as perfluorodecyltrichlorosilane (FDTS), n-decyltrichlorosilane (DTS), and 6-phenylhexyl -trichlorosilane (PTS), as shown in Fig. 27 (e and f). In particular, attractive capillary action by PTS treated surface resulted in better polymer alignment on the nanogrooved surface and by tilting the

tunnel system film morphology was further improved. With optimized OFET channel length (140 μm), mobility of such oriented PCDTPT thin film reached up to 36.3 cm^2/Vs. Although sequential development of this technique has been mainly demonstrated with PCDTPT, improved mobility in other CPs were also demonstrated through this technique which confirms its universality. [164,165] This technique is suitable for material research and to explore high charge transport property of new CPs. However, Slow device fabrication process and complex experimental setup are the bottlenecks in the way to its commercialization.

3.5 Directional Epitaxial Crystallization

Crystalline growth of a guest material on a crystalline surface (host crystal) following its crystallographic orientation is termed as epitaxy, where the key to induce crystallinity is the control of the solidification process. Epitaxial growth of CPs have been much explored in past and its application to orient semiconducting polymer was first demonstrated by Brinkmann and coworkers and has been reviewed by him in detail.[10,166–170] They fabricated the large area oriented P3HT films by directional solidification on 1,3,5-trichlorobenzene (TCB) acting as a crystallizable aromatic solvent shown in. Concisely, on pre-casted P3HT thin film, TCB powder was deposited and firmly covered with a glass coverslip followed by heating above the melting temperature of TCB, where the molten TCB acts as solvent for P3HT. In continuation, gentle movement of the system towards colder region imitated directional crystallization of TCB simultaneously increasing concentration of P3HT in the remaining liquid led to its aggregation and crystallization. After complete crystallization of TCB, it acted as the substrate for epitaxy, which was finally sublimated in a vacuum oven leaving oriented P3HT on the substrate. Further development to enhance thin film characteristics and its application to other conducting polymer systems were extensively report by

the same group.[171–174] They have also reported enhancement in macromolecular orientation by improvising the film fabrication setup, **Fig. 28**. In place of melting whole film simultaneously (standard Directional Epitaxial Crystallization (DCE)), a local-melting technique was utilized in the improved-DCE technique, which provided better control on the rate of TCB crystal growth.[55] Moreover the PTFE coated substrate allowed guided crystal growth of TCB. Consequently oriented P3HT thin film with (DR ≈ 10) was obtained.

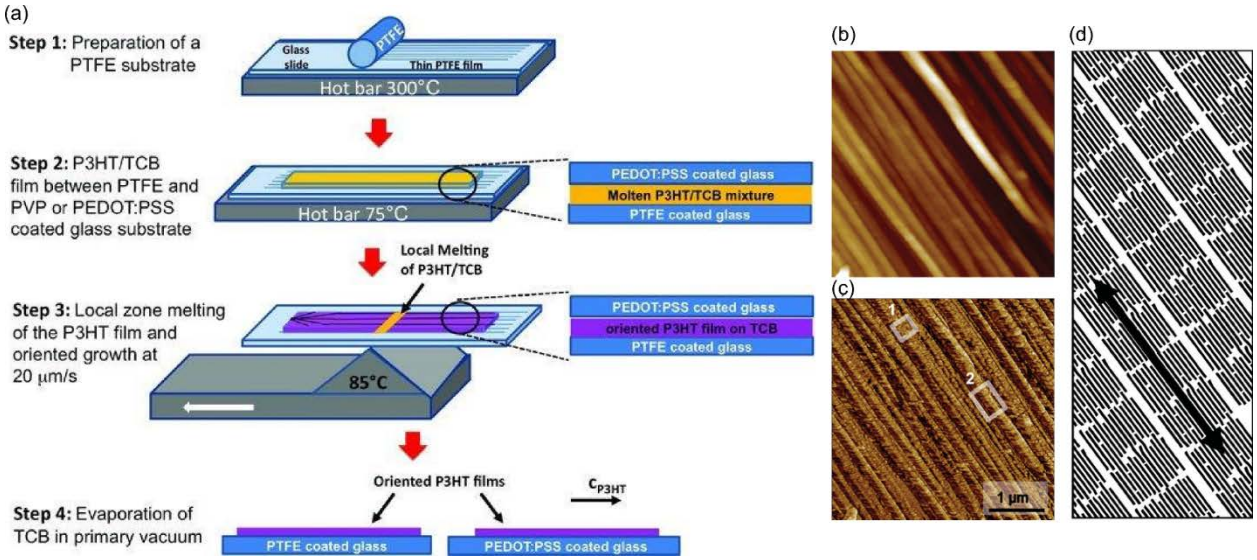

Fig. 28. (a) Schematic description of the different steps involved in fabrication of oriented P3HT films by the improved directional epitaxial crystallization technique. (Reprinted with permission from ref. 55. Copyright (2011), John Wiley and Sons.). AFM images of directionally crystallized P3HT thin films (initial directional epitaxial crystallization technique): (b) height mode and (c) phase mode. The box labeled 1 outlines a region with equiaxed crystallites. The box labeled 2 outlines a region with elongated crystallites. The polymer-chain axis is parallel to the fiber axis, as indicated by the arrow in (d). (Reprinted with permission from Ref. 16. Copyright (2009), John Wiley and Sons.)

Application of oriented P3HT film (obtained through standard DEC) (Fig. 28 (b – d)) in OFETs was first reported by Salleo group to understand the charge-transport mechanism in oriented thin films.[16] High mobility anisotropy of $\mu_{\parallel}/\mu_{\perp}$ >10 was reported with favorable charge transport along

the polymer backbone with mobility > 10^{-2} $cm^2/V.s$. Reason for this anisotropic charge transport was attributed to the larger transport barrier due to grain boundaries between fibers compared to boundaries along the fiber. Further, Muller et al. have demonstrated one-step fabrication of oriented thin films directly from solution, by using a second carrier solvent (chlorobenzene) along with TCB to spin-coat the P3HT thin film. On solidification, spherulitic structure of P3HT was observed on TCB crystals and through its subsequent sublimation oriented thin film was obtained.[175] This technique can be a better tool to fabricate oriented thin films of less crystalline materials.

3.6 Dynamic-template-directed orientation

As the name suggests, in this technique the dynamic host template can alter its surface structure to maximize the favorable interaction with the guest system. Mohammadi et al. have reported this technique to orient CPs.[176–178] They prepared the dynamic-template setup by infiltrating nonporous anodized aluminum oxide (AAO) membrane placed on a glass substrate with an ionic liquid (IL) as shown in **Fig.29**. To fabricate the thin film, polymer solution (in volatile solvent) was place on the IL-template and sheared by an inclined blade, while the IL retained its place due to capillary force imparted by AAO nano-pores. Finally the solid film was transferred on the desired substrate.[176] Although the coating head was similar to that of solution-shearing technique, orientation was mainly guided by the electrostatic interaction between IL and CP at the interface. A maximum DR of 10.1 was obtained for thinnest film (~10 nm thick) of DPPT-TT, which was decreased by further increase in film thickness due to higher probability of bulk nucleation in the polymer solution compared to IL-template induced nucleation. Albeit, for such low thickness hampered mobility along with non-ideal downward kinks in the transfer characteristics was

observed, which was attributed to mechanical damages created in the film. At optimum film thickness (~200 nm) maximum mobility along backbone orientation reached up to 2.24 cm^2/Vs (with $\mu_{\parallel}/\mu_{\perp} \approx 3$). Very recently the same group have demonstrated synergistic dynamic templating effect of IL and polymer matrix (elastic polyvinylidene fluoride-co-hexafluoropropylene(e-P(VDF:HFP))), where IL and polymer matrix, interacts with the conjugated backbone and the alkyl side chain, respectively.[177] The thin film of IL-polymer matrix acted as both template and ion-gel get dielectric for bottom-gate top-contact OFET resulted in enhanced mobility (up to 12.5$cm^2/V.s$ along backbone orientation with $\mu_{\parallel}/\mu_{\perp} \approx 2$ for DPP-BTz). The freedom of changing the coating speed without compromising the film's transport property, qualifies this technique for swift fabrication of large scale printed electronics. However, mechanical damage to the thin film during transfer still needs to be addressed.

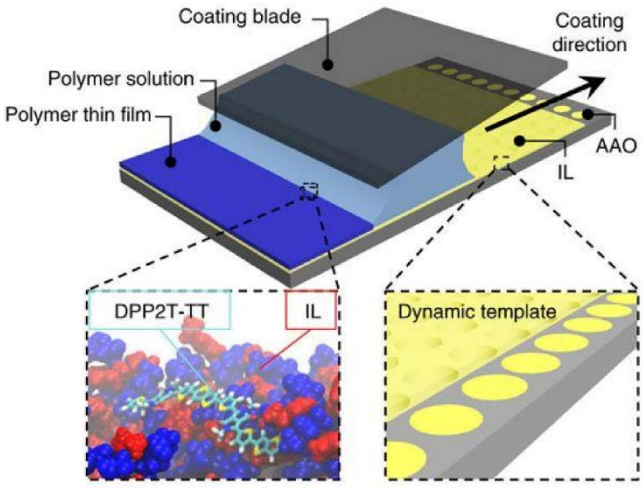

Fig. 29. Schematic (not to scale) of film coating on the IL/AAO dynamic template. The black arrow indicates the coating direction. (Reprinted from 176.)

4. Conclusion and future prospects

The unique quasi 1-dimensionality and planar molecular structure of CPs results in extended π-conjugation.[179] To exploit the utmost performance of a CP based electronic devices, their unidirectional orientation at macroscopic scale and macromolecular conformation/packing is equally important. This high interconnectivity through orientation enables high intra and inter molecular interactions and lowers the energetic barriers for charge carriers; therefore, facilitating high charge carrier transport through main chains assisted by hopping through the tie-chains and π-π stacking.[11,142] Optical and electrical anisotropy are a consequence of the molecular orientation of CPs parallel to channel maximize the carrier transport in OFETs.

In this article, various techniques to orient the CPs have been reviewed. Discussion on each of the techniques has been started from the initial report followed by a brief description of the physical phenomena occurring during the film fabrication to understanding the different parameters governing orientation. Further, the recent progress, advantages and the existing challenges are discussed. In comparison to the previous progress reports,[10,180] our present review incorporated recent advancement made till date and included many new solution processable methods with especial consideration about the solution based thin film fabrication methods like FTM, film Compression at surface of ionic liquid, dynamic-template-directed orientation, etc. Major emphasis has been given on the charge transport anisotropy in OFETs arising from the orientation or conformational changes.

Orientation in CPs through friction transfer and mechanical rubbing is a low-cost and powerful technique. However, these techniques lags in achieving favorable edge-on orientation on hydrophobic surface that results in lower field effect mobility.[44] Other orientation techniques like

directional epitaxial crystallization and strain alignment need multistep processes, which are not suitable for the large area roll-to-roll fabrication. Orientation techniques like dip coating, off-center spin coating and directional solvent evaporation have demonstrated high field effect mobilites but their use seems to be limited small area laboratory-scale.[78,128,161,164,165] To attain the goal of the roll-to-roll mass fabrication of high performance printed electronics, various solution processable techniques have demonstrated, such as wire-bar coating, solution shearing, FTM and dynamic-template-directed technique. Demonstration of high performance large area stretchable organic thin film by modified solution shearing symbolize the great futuristic possibilities for the stretchable and wearable electronics.[115] FTM is a promising technique to prepare large area oriented film on liquid substrate and can be utilized for layer-by-layer coating and high performance OFETs.[137,142,157] However, good solubility of the CPs is essential in FTM as the orientation rely on the self-assembly of the CPs. Dynamic-template-directed technique qualifies swift fabrication of the large area oriented thin film but device robustness and stability issues need to be addressed.[176,177]

Each technique has their own associated merits and demerits and judicious selection of a suitable technique can be done with ease. However, industrial application of such methods to prepared oriented films stills needs to be realized, for printed electronics with the environment-friendly processes. In this context, future research towards the application of non-halogenated solvents for oriented thin film fabrication bears a great potential. It is believed that in the near future we may likely to witness printable film fabrication strategies that can enable roll-to-roll fabrication of highly oriented film of CPs.

Acknowledgement: This work was partially supported by Grant-in-Aid for Scientific Research (c), (Grant Number 15K05989). Authors are thankful to Kyushu Institute of Technology for providing research facilities.

References

1 T. Someya, T. Sekitani, S. Iba, Y. Kato, H. Kawaguchi and T. Sakurai, *PNAS*, 2004, **98**, 4835–4840.

2 T. Sekitani, U. Zschieschang, H. Klauk and T. Someya, *Nat. Mater.*, 2010, **9**, 1015–1022.

3 C. D. Dimitrakopoulos and P. R. L. Malenfant, *Adv. Mater.*, 2002, **14**, 99–117.

4 A. Facchetti, *Chem. Mater.*, 2011, **23**, 733–758.

5 H. Sirringhaus, *Adv. Mater.*, 2014, 26, 1319–1335.

6 G. H. Gelinck, H. E. a Huitema, E. van Veenendaal, E. Cantatore, L. Schrijnemakers, J. B. P. H. van der Putten, T. C. T. Geuns, M. Beenhakkers, J. B. Giesbers, B.-H. Huisman, E. J. Meijer, E. M. Benito, F. J. Touwslager, A. W. Marsman, B. J. E. van Rens and D. M. de Leeuw, *Nat. Mater.*, 2004, **3**, 106–110.

7 H. Yang, S. W. Lefevre, C. Y. Ryu and Z. Bao, *Appl. Phys. Lett.*, 2007, **90**, 172116.

8 J. F. Chang, B. Sun, D. W. Breiby, M. M. Nielsen, T. I. Sölling, M. Giles, I. McCulloch and H. Sirringhaus, *Chem. Mater.*, 2004, **16**, 4772–4776.

9 H. N. Tsao, D. Cho, J. W. Andreasen, A. Rouhanipour, D. W. Breiby, W. Pisula and K. Müllen, *Adv. Mater.*, 2009, **21**, 209–212.

10 M. Brinkmann, L. Hartmann, L. Biniek, K. Tremel and N. Kayunkid, *Macromol. Rapid Commun.*, 2014, **35**, 9–26.

11 E. J. W. Crossland, K. Tremel, F. Fischer, K. Rahimi, G. Reiter, U. Steiner and S. Ludwigs, *Adv. Mater.*, 2012, **24**, 839–844.

12 H. Sirringhaus, *Adv. Mater.*, 2005, **17**, 2411–2425.

13 A. Salleo, *Mater. Today*, 2007, **10**, 38–45.

14 M. Nikolka and H. Sirringhaus, in *Conjugated Polymers*, CRC Press, 2019, pp. 1–20.

15 A. F. Paterson, S. Singh, K. J. Fallon, T. Hodsden, Y. Han, B. C. Schroeder, H. Bronstein, M. Heeney, I. McCulloch and T. D. Anthopoulos, *Adv. Mater.*, 2018, **30**, 1801079.

16 L. H. Jimison, M. F. Toney, I. McCulloch, M. Heeney and A. Salleo, *Adv. Mater.*, 2009, **21**, 1568–1572.

17 H. Sirringhaus, P. J. Brown, R. H. Friend, M. M. Nielsen, K. Bechgaard, B. M. W. Langeveld-Voss, A. J. H. Spiering, R. A. J. Janssen, E. W. Meijer, P. Herwig and D. M. De Leeuw, *Nature*, 1999, **401**, 685–688.

18 J. R. Tumbleston, B. A. Collins, L. Yang, A. C. Stuart, E. Gann, W. Ma, W. You and H. Ade, *Nat. Photonics*, 2014, **8**, 385–391.

19 N. I. C. Alignment, H. T. N. Defined and N. Lithography, *ACS Nano*, 2009, **3**, 3085–3090.

20 J. Liu, Y. Sun, X. Gao, R. Xing, L. Zheng, S. Wu, Y. Geng and Y. Han, *Langmuir*, 2011, **27**, 4212–4219.

21 J. Ma, K. Hashimoto, T. Koganezawa and K. Tajima, *J. Am. Chem. Soc.*, 2013, **135**, 9644–9647.

22 J. Ma, K. Hashimoto, T. Koganezawa and K. Tajima, *Chem. Commun.*, 2014, **50**, 3627.

23 F. Wang, K. Nakano, H. Yoshida, K. Hashimoto, H. Segawa, C.-S. Hsu and K. Tajima, *J. Mater. Chem. A*, 2018, **6**, 22889–22898.

24 F. Wang, K. Hashimoto, H. Segawa and K. Tajima, *ACS Appl. Mater. Interfaces*, 2018, **10**, 8901–8908.

25 M. L. Chabinyc, *Polym. Rev.*, 2008, **48**, 463–492.

26 R. Noriega, J. Rivnay, K. Vandewal, F. P. V Koch, N. Stingelin, P. Smith, M. F. Toney and A. Salleo, *Nat. Mater.*, 2013, **12**, 1038–44.

27 M. L. Chabinyc, M. F. Toney, R. J. Kline, I. McCulloch and M. Heeney, *J. Am. Chem. Soc.*, 2007, **129**, 3226–3237.

28 J. Rivnay, S. C. B. Mannsfeld, C. E. Miller, A. Salleo and M. F. Toney, *Chem. Rev.*, 2012.

29 I. Osaka and K. Takimiya, *Polymer (Guildf).*, 2015, **59**, A1–A15.

30 S. Nagamatsu, W. Takashima, K. Kaneto, Y. Yoshida, N. Tanigaki, K. Yase and K. Omote, *Macromolecules*, 2003, **36**, 5252–5257.

31 S. Nagamatsu, M. Misaki, M. Chikamatsu, T. Kimura, Y. Yoshida, R. Azumi, N. Tanigaki and K. Yase, *J. Phys. Chem. B*, 2007, **111**, 4349–4354.

32 J. Als-Nielsen and D. McMorrow, *Elements of Modern X-ray Physics*, John Wiley & Sons, Inc., Hoboken, NJ, USA, 2011.

33 M. M. Nahid, E. Gann, L. Thomsen and C. R. McNeill, *Eur. Polym. J.*, 2016, 81, 532–554.

34 J. C. Wittmann and P. Smith, *Nature*, 1991, **352**, 414–417.

35 F. Motamedi, K. J. Ihn, D. Fenwick, J. C. C. Wittmann and P. Smith, *J. Polym. Sci. Part B Polym. Phys.*, 1994, **32**, 453–457.

36 S. Machida, M. Tanikatsu, A. Itaya and N. Ikeda, *J. Cryst. Growth*, 2017, **468**, 781–787.

37 F. Xu, D. Lin, W. Xia, W. Cao, Q. Chen, Q. Zhang and G. Zhu, *Org. Electron.*, 2019, **64**, 86–91.

38 W. Xia, Q. Chen, J. Zhang, H. Wang, Q. Cheng, Y. Jiang and G. Zhu, *Appl. Surf. Sci.*, 2018, **437**, 209–216.

39 M. Misaki, Y. Ueda, S. Nagamatsu, Y. Yoshida, N. Tanigaki and K. Yase, *Macromolecules*, 2004, **37**, 6926–6931.

40 M. Misaki, S. Nagamatsu, M. Chikamatsu, Y. Yoshida, R. Azumi, N. Tanigaki, Y. Ueda and K. Yase, *Polym. J.*, 2007, **39**, 1306–1311.

41 N. Tanigaki, K. Yase, A. Kaito and K. Ueno, *Polymer (Guildf).*, 1995, **36**, 2477–2480.

42 N. Tanigaki, K. Yase and A. Kaito, *Thin Solid Films*, 1996, **273**, 263–266.

43 Y. Hosokawa, M. Misaki, S. Yamamoto, M. Torii, K. Ishida and Y. Ueda, *Appl. Phys. Lett.*, 2012, **100**, 203305.

44 N. Kumari, A. S. M. Tripathi, S. Sadakata, M. Pandey, S. Nagamatsu, S. Hayase and S. S. Pandey, *Org. Electron.*, 2019, **68**, 221–229.

45 S. Nagamatsu, W. Takashima, K. Kaneto, Y. Yoshida, N. Tanigaki and K. Yase, *Appl. Phys. Lett.*, 2004, **84**, 4608–4610.

46 N. Tanigaki, S. Nagamatsu, W. Takashima and Y. Yoshida, *Thin Solid Films*, 2009, **518**, 853–856.

47 T. Kanetake, K. Ishikawa, T. Koda, Y. Tokura and K. Takeda, *Appl. Phys. Lett.*, 1987, **51**, 1957–1959.

48 M. Hamaguchi and K. Yoshino, *Appl. Phys. Lett.*, 1995, **67**, 3381–3383.

49 M. Hamaguchi and K. Yoshino, *Polym. Adv. Technol.*, 1997, **8**, 399–402.

50 M. F. Toney, T. P. Russell, J. A. Logan, H. Kikuchi, J. M. Sands and S. K. Kumar, *Nature*, 1995, 374, 709–711.

51 N. A. J. M. van Aerle and A. J. W. Tol, *Macromolecules*, 1994, **27**, 6520–6526.

52 N. A. J. M. van Aerle, M. Barmentlo and R. W. J. Hollering, *J. Appl. Phys.*, 1993, **74**, 3111–3120.

53 a Bolognesi, C. Botta, M. Martinelli and W. Porzio, *Org. Electron.*, 2000, **1**, 27–32.

54 H. Heil, T. Finnberg, N. Von Malm, R. Schmechel and H. Von Seggern, *J. Appl. Phys.*, 2003, **93**, 1636–1641.

55 L. Hartmann, K. Tremel, S. Uttiya, E. Crossland, S. Ludwigs, N. Kayunkid, C. Vergnat and M. Brinkmann, *Adv. Funct. Mater.*, 2011, **21**, 4047–4057.

56 L. Biniek, N. Leclerc, T. Heiser, R. Bechara and M. Brinkmann, *Macromolecules*, 2013, **46**, 4014–4023.

57 K. Tremel, F. S. U. Fischer, N. Kayunkid, R. Di Pietro, R. Tkachov, A. Kiriy, D. Neher, S. Ludwigs and M. Brinkmann, *Adv. Energy Mater.*, 2014, **4**, 1–13.

58 L. Biniek, S. Pouget, D. Djurado, E. Gonthier, K. Tremel, N. Kayunkid, E. Zaborova, N. Crespo-Monteiro, O. Boyron, N. Leclerc, S. Ludwigs and M. Brinkmann, *Macromolecules*, 2014, **47**, 3871–3879.

59 A. Hamidi-Sakr, L. Biniek, S. Fall and M. Brinkmann, *Adv. Funct. Mater.*, 2016, **26**, 408–420.

60 A. Hamidi-Sakr, L. Biniek, J.-L. Bantignies, D. Maurin, L. Herrmann, N. Leclerc, P. Lévêque, V. Vijayakumar, N. Zimmermann and M. Brinkmann, *Adv. Funct. Mater.*, 2017, **27**, 1700173.

61 D. Kajiya, S. Ozawa, T. Koganezawa and K. I. Saitow, *J. Phys. Chem. C*, 2015, **119**, 7987–7995.

62 D. Kajiya, T. Koganezawa and K. I. Saitow, *J. Phys. Chem. C*, 2016, **120**, 23351–23357.

63 T. Kushida, T. Nagase and H. Naito, *Org. Electron.*, 2011, **12**, 2140–2143.

64 T. Kushida, T. Nagase and H. Naito, *Appl. Phys. Lett.*, 2014, **104**, 093304.

65 P. Dyreklev, M. Berggren, O. Inganäs, M. R. Andersson, O. Wennerström and T. Hjertberg, *Adv. Mater.*, 1995, **7**, 43–45.

66 B. O'Connor, R. J. Kline, B. R. Conrad, L. J. Richter, D. Gundlach, M. F. Toney and D. M. DeLongchamp, *Adv. Funct. Mater.*, 2011, **21**, 3697–3705.

67 B. T. O'Connor, O. G. Reid, X. Zhang, R. J. Kline, L. J. Richter, D. J. Gundlach, D. M. Delongchamp, M. F. Toney, N. Kopidakis and G. Rumbles, *Adv. Funct. Mater.*, 2014, **24**, 3422–3431.

68 B. O'Connor, E. P. Chan, C. Chan, B. R. Conrad, L. J. Richter, R. J. Kline, M. Heeney, I. McCulloch, C. L. Soles and D. M. DeLongchamp, *ACS Nano*, 2010, **4**, 7538–7544.

69 X. Xue, G. Chandler, X. Zhang, R. J. Kline, Z. Fei, M. Heeney, P. J. Diemer, O. D. Jurchescu and B. T. O'connor, *ACS Appl. Mater. Interfaces*, 2015, **7**, 26726–26734.

70 J. Soeda, H. Matsui, T. Okamoto, I. Osaka, K. Takimiya and J. Takeya, *Adv. Mater.*, 2014, **26**, 6430–6435.

71 Y. Yamashita, F. Hinkel, T. Marszalek, W. Zajaczkowski, W. Pisula, M. Baumgarten, H. Matsui, K. Müllen and J. Takeya, *Chem. Mater.*, 2016, **28**, 420–424.

72 M. Sasaki, Y. Yamashita, H. Matsui, Y. Oshima and J. Takeya, *Microscopy*, 2019, **68**, 167–173.

73 M. J. Lee, D. Gupta, N. Zhao, M. Heeney, I. McCulloch and H. Sirringhaus, *Adv. Funct. Mater.*, 2011, **21**, 932–940.

74 G. Giri, D. M. DeLongchamp, J. Reinspach, D. A. Fischer, L. J. Richter, J. Xu, S. Benight, A. Ayzner, M. He, L. Fang, G. Xue, M. F. Toney and Z. Bao, *Chem. Mater.*, 2015, **27**, 2350–2359.

75 X. Gu, L. Shaw, K. Gu, M. F. Toney and Z. Bao, *Nat. Commun.*, 2018, **9**, 534.

76 T. Umeda, D. Kumaki and S. Tokito, *J. Appl. Phys.*, 2009, **105**, 024516.

77 S. G. Bucella, A. Luzio, E. Gann, L. Thomsen, C. R. McNeill, G. Pace, A. Perinot, Z. Chen, A. Facchetti and M. Caironi, *Nat. Commun.*, 2015, **6**, 8394.

78 S. Wang, A. Kiersnowski, W. Pisula and K. Müllen, *J. Am. Chem. Soc.*, 2012, **134**, 4015–4018.

79 S. Schott, E. Gann, L. Thomsen, S.-H. Jung, J.-K. Lee, C. R. McNeill and H. Sirringhaus, *Adv. Mater.*, 2015, **27**, 7356–7364.

80 Y. Jiang, J. Chen, Y. Sun, Q. Li, Z. Cai, J. Li, Y. Guo, W. Hu and Y. Liu, *Adv. Mater.*, 2019, **31**, 1805761.

81 R. D. Deegan, O. Bakajin, T. F. Dupont, G. Huber, S. R. Nagel and T. A. Witten, *Phys. Rev. E*, 2000, **62**, 756–765.

82 L. Landau and B. Levich, *Dyn. Curved Front.*, 1988, 141–153.

83 M. Le Berre, Y. Chen and D. Baigl, *Langmuir*, 2009, **25**, 2554–2557.

84 M. Faustini, B. Louis, P. A. Albouy, M. Kuemmel and D. Grosso, *J. Phys. Chem. C*, 2010, **114**, 7637–7645.

85 J. Lee, A.-R. Han, J. Kim, Y. Kim, J. H. Oh and C. Yang, *J. Am. Chem. Soc.*, 2012, **134**, 20713–20721.

86 J. Lee, A.-R. Han, H. Yu, T. J. Shin, C. Yang and J. H. Oh, *J. Am. Chem. Soc.*, 2013, **135**, 9540–9547.

87 H. L. Yi, C. H. Wu, C. I. Wang and C. C. Hua, *Macromolecules*, 2017, **50**, 5498–5509.

88 L. Janasz, D. Chlebosz, M. Gradzka, W. Zajaczkowski, T. Marszalek, K. Müllen, J. Ulanski, A. Kiersnowski and W. Pisula, *J. Mater. Chem. C*, 2016, **4**, 11488–11498.

89 A. R. Aiyar, J.-I. Hong, J. Izumi, D. Choi, N. Kleinhenz and E. Reichmanis, *ACS Appl. Mater. Interfaces*, 2013, **5**, 2368–2377.

90 M. Chang, J. Lee, N. Kleinhenz, B. Fu and E. Reichmanis, *Adv. Funct. Mater.*, 2014, **24**, 4457–4465.

91 D. Quéré, *Annu. Rev. Fluid Mech.*, 1999, **31**, 347–384.

92 J.-M. Verilhac, G. LeBlevennec, D. Djurado, F. Rieutord, M. Chouiki, J.-P. Travers and A. Pron, *Synth. Met.*, 2006, **156**, 815–823.

93 E. Meyer and H.-G. Braun, *J. Phys. Condens. Matter*, 2005, **17**, S623–S635.

94 G. Wang, J. Swensen, D. Moses and A. J. Heeger, *J. Appl. Phys.*, 2003, **93**, 6137–6141.

95 S. Wang, W. Pisula and K. Müllen, *J. Mater. Chem.*, 2012, **22**, 24827.

96 M. Li, C. An, W. Pisula and K. Müllen, *Small*, 2014, **10**, 1926–1931.

97 S. R. Tseng, H. F. Meng, K. C. Lee and S. F. Horng, *Appl. Phys. Lett.*, 2008, **93**, 153308.

98 A. Pierre, M. Sadeghi, M. M. Payne, A. Facchetti, J. E. Anthony and A. C. Arias, *Adv. Mater.*, 2014, **26**, 5722–5727.

99 Y.-H. Lee, P.-T. Tsai, C.-J. Chang, H.-F. Meng, S.-F. Horng, H.-W. Zan, H.-C. Lin, H.-C. Liu, M.-R. Tseng and H.-C. Yeh, *AIP Adv.*, 2016, **6**, 115006.

100 P. H. Chu, N. Kleinhenz, N. Persson, M. McBride, J. L. Hernandez, B. Fu, G. Zhang and E. Reichmanis, *Chem. Mater.*, 2016, **28**, 9099–9109.

101 Shear force, https://en.wikipedia.org/wiki/Shear_force, (accessed 31 July 2019).

102 Shear stress, https://en.wikipedia.org/wiki/Shear_stress, (accessed 31 July 2019).

103 R. S. Sánchez-Carrera, S. Atahan, J. Schrier and A. Aspuru-Guzik, *J. Phys. Chem. C*, 2010, **114**, 2334–2340.

104 J. Cornil, D. Beljonne, J.-P. Calbert and J.-L. Brédas, *Adv. Mater.*, 2001, **13**, 1053–1067.

105 Y. Diao, B. C. K. Tee, G. Giri, J. Xu, D. H. Kim, H. A. Becerril, R. M. Stoltenberg, T. H. Lee, G. Xue, S. C. B. Mannsfeld and Z. Bao, *Nat. Mater.*, 2013, **12**, 665–671.

106 H. A. Becerril, M. E. Roberts, Z. Liu, J. Locklin and Z. Bao, *Adv. Mater.*, 2008, **20**, 2588–2594.

107 H. Yabu and M. Shimomura, *Adv. Funct. Mater.*, 2005, **15**, 575–581.

108 M. Karakawa, M. Chikamatsu, Y. Yoshida, M. Oishi, R. Azumi and K. Yase, *Appl. Phys. Express*, 2008, **1**, 061802.

109 G. Allegra and S. V. Meille, in *Interphases and Mesophases in Polymer Crystallization III*, Springer-Verlag, Berlin/Heidelberg, pp. 87–135.

110 A. Keller and S. Z. D. Cheng, *Polymer (Guildf).*, 1998, **39**, 4461–4487.

111 W. Y. Lee, G. Giri, Y. Diao, C. J. Tassone, J. R. Matthews, M. L. Sorensen, S. C. B. Mannsfeld, W. C. Chen, H. H. Fong, J. B. H. Tok, M. F. Toney, M. He and Z. Bao, *Adv. Funct. Mater.*, 2014, **24**, 3524–3534.

112 J. Shin, T. R. Hong, T. W. Lee, A. Kim, Y. H. Kim, M. J. Cho and D. H. Choi, *Adv. Mater.*, 2014, **26**, 6031–6035.

113 D. Wu, M. Kaplan, H. W. Ro, S. Engmann, D. A. Fischer, D. M. DeLongchamp, L. J. Richter, E. Gann, L. Thomsen, C. R. McNeill and X. Zhang, *Chem. Mater.*, 2018, **30**, 1924–1936.

114 J. P. Rolland, R. M. Van Dam, D. A. Schorzman, S. R. Quake and J. M. DeSimone, *J. Am. Chem. Soc.*, 2004, **126**, 2322–2323.

115 J. Xu, H.-C. Wu, C. Zhu, A. Ehrlich, L. Shaw, M. Nikolka, S. Wang, F. Molina-Lopez, X. Gu, S. Luo, D. Zhou, Y.-H. Kim, G.-J. N. Wang, K. Gu, V. R. Feig, S. Chen, Y. Kim, T. Katsumata, Y.-Q. Zheng, H. Yan, J. W. Chung, J. Lopez, B. Murmann and Z. Bao, *Nat. Mater.*, 2019, **18**, 594–601.

116 J. Xu, S. Wang, G.-J. N. Wang, C. Zhu, S. Luo, L. Jin, X. Gu, S. Chen, V. R. Feig, J. W. F. To, S. Rondeau-Gagné, J. Park, B. C. Schroeder, C. Lu, J. Y. Oh, Y. Wang, Y.-H. Kim, H. Yan, R. Sinclair, D. Zhou, G. Xue, B. Murmann, C. Linder, W. Cai, J. B.-H. Tok, J. W. Chung and Z. Bao, *Science (80-.).*, 2017, **355**, 59–64.

117 Z. Zhang, B. Peng, X. Ji, K. Pei and P. K. L. Chan, *Adv. Funct. Mater.*, 2017, **27**, 1703443.

118 B. Dan, G. C. Irvin and M. Pasquali, *ACS Nano*, 2009, **3**, 835–843.

119 J. Ouyang, T.-F. Guo, Y. Yang, H. Higuchi, M. Yoshioka and T. Nagatsuka, *Adv. Mater.*, 2002, **14**, 915.

120 C. E. Murphy, L. Yang, S. Ray, L. Yu, S. Knox and N. Stingelin, *J. Appl. Phys.*, 2011, **110**, 093523.

121 D. Khim, H. Han, K. J. Baeg, J. Kim, S. W. Kwak, D. Y. Kim and Y. Y. Noh, *Adv. Mater.*, 2013, **25**, 4302–4308.

122 D. Khim, G.-S. Ryu, W.-T. Park, H. Kim, M. Lee and Y.-Y. Noh, *Adv. Mater.*, 2016, **28**, 2752–2759.

123 Y. Yuan, G. Giri, A. L. Ayzner, A. P. Zoombelt, S. C. B. Mannsfeld, J. Chen, D. Nordlund, M. F. Toney, J. Huang and Z. Bao, *Nat. Commun.*, 2014, **5**, 3005.

124 H. Wang, L. Chen, R. Xing, J. Liu and Y. Han, *Langmuir*, 2015, **31**, 469–479.

125 R. Matsidik, H. Komber, A. Luzio, M. Caironi and M. Sommer, *J. Am. Chem. Soc.*, 2015, **137**, 6705–6711.

126 R. Steyrleuthner, M. Schubert, I. Howard, B. Klaumünzer, K. Schilling, Z. Chen, P. Saalfrank, F. Laquai, A. Facchetti and D. Neher, *J. Am. Chem. Soc.*, 2012, **134**, 18303–18317.

127 N. K. Kim, S. Y. Jang, G. Pace, M. Caironi, W. T. Park, D. Khim, J. Kim, D. Y. Kim and Y. Y. Noh, *Chem. Mater.*, 2015, **27**, 8345–8353.

128 N. K. Kim, E. S. Shin, Y. Y. Noh and D. Y. Kim, *Org. Electron.*, 2018, **55**, 6–14.

129 E.-S. Shin and Y.-Y. Noh, *Org. Electron.*, 2018, **53**, 111–116.

130 C. M. Hansen, *Hansen Solubility Parameters*, CRC Press, 2007.

131 L. Van Tho, W. T. Park, E. Y. Choi and Y. Y. Noh, *Appl. Phys. Lett.*, 2017, **110**, 163303.

132 J. Huang, J. H. Carpenter, C. Z. Li, J. S. Yu, H. Ade and A. K.-Y. Jen, *Adv. Mater.*, 2016, **28**, 967–974.

133 T. Morita, V. Singh, S. Nagamatsu, S. Oku, W. Takashima and K. Kaneto, *Appl. Phys. Express*, 2009, **2**, 12–15.

134 D. S. Yang, M. Barłóg, J. Park, K. Chung, A. Shanker, J. Sun, J. Kang, K. Lee, M. Al-Hashimi and J. Kim, *ACS Omega*, 2018, **3**, 14807–14813.

135 A. Dauendorffer, S. Nagamatsu, W. Takashima and K. Kaneto, *Jpn. J. Appl. Phys.*, 2012, **51**, 055802.

136 T. Ohtomo, K. Hashimoto, H. Tanaka, Y. Ohmori, M. Ozaki and H. Kajii, *Org. Electron.*, 2016, **32**, 213–219.

137 M. Pandey, S. Sadakata, S. Nagamatsu, S. S. Pandey, S. Hayase and W. Takashima, *Synth. Met.*, 2017, **227**, 29–36.

138 R. K. Pandey, W. Takashima, S. Nagamatsu, A. Dauendorffer, K. Kaneto and R. Prakash, *J. Appl. Phys.*, 2013, **114**, 054309.

139 D. Arnaud, R. K. Pandey, S. Miyajima, S. Nagamatsu, R. Prakash, W. Takashima, S. Hayase and K. Kaneto, *Trans. Mater. Res. Soc. Japan*, 2013, **38**, 305–308.

140 M. Pandey, S. S. Pandey, S. Nagamatsu, S. Hayase and W. Takashima, *J. Nanosci. Nanotechnol.*, 2017, **17**, 1915–1922.

141 M. Pandey, S. Nagamatsu, S. S. Pandey, S. Hayase and W. Takashima, *Org. Electron.*, 2016, **38**, 115–120.

142 M. Pandey, A. Gowda, S. Nagamatsu, S. Kumar, W. Takashima, S. Hayase and S. S. Pandey, *Adv. Mater. Interfaces*, 2018, **5**, 1700875.

143 A. Nawaz, A. Kumar and I. A. Hümmelgen, *Org. Electron.*, 2017, **51**, 94–102.

144 M. Pandey, S. S. Pandey, S. Nagamatsu, S. Hayase and W. Takashima, *Thin Solid Films*, 2016, **619**, 125–130.

145 A. Nawaz, A. C. B. Tavares, T. Trang Do, B. B. Patil, P. Sonar and I. A. Hümmelgen, *Flex. Print. Electron.*, 2018, **3**, 015006.

146 M. Pandey, S. S. Pandey, S. Nagamatsu, S. Hayase and W. Takashima, *Org. Electron.*, 2017, **43**, 240–246.

147 M. Pandey, S. Nagamatsu, S. S. Pandey, S. Hayase and W. Takashima, *J. Phys. Conf. Ser.*, 2016, **704**, 012005.

148 L. Korson, W. Drost-Hansen and F. J. Millero, *J. Phys. Chem.*, 1969, **73**, 34–39.

149 J. B. Segur and H. E. Oberstar, *Ind. Eng. Chem.*, 1951, **43**, 2117–2120.

150 C. Cragoe, *Properties of ethylene glycol and its aqueous solutions*, Cooperative Fuel Research Committee of the Cooperative Research Council, New York, 1943.

151 R. E. Maples, *Petroleum refinery process economics*, PennWell Books, 1993.

152 M. Pandey, S. Nagamatsu, W. Takashima, S. S. Pandey and S. Hayase, *J. Phys. Chem. C*, 2017, **121**, 11184–11193.

153 R. J. Kline, D. M. DeLongchamp, D. A. Fischer, E. K. Lin, L. J. Richter, M. L. Chabinyc, M. F. Toney, M. Heeney and I. McCulloch, *Macromolecules*, 2007, **40**, 7960–7965.

154 D. M. DeLongchamp, R. J. Kline, Y. Jung, E. K. Lin, D. A. Fischer, D. J. Gundlach, S. K. Cotts, A. J. Moad, L. J. Richter, M. F. Toney, M. Heeney and I. McCulloch, *Macromolecules*, 2008, **41**, 5709–5715.

155 J. Y. Na, M. Kim and Y. D. Park, *J. Phys. Chem. C*, 2017, **121**, 13930–13937.

156 J. Chang, Z. Lin, J. Li, S. L. Lim, F. Wang, G. Li, J. Zhang and J. Wu, *Adv. Electron. Mater.*, 2015, **1**, 1500036.

157 A. S. M. Tripathi, M. Pandey, S. Sadakata, S. Nagamatsu, W. Takashima, S. Hayase and S. S. Pandey, *Appl. Phys. Lett.*, 2018, **112**, 123301.

158 A. S. M. Tripathi, N. Kumari, S. Nagamatsu, S. Hayase and S. S. Pandey, *Org. Electron.*, 2019, **65**, 1–7.

159 H.-R. Tseng, L. Ying, B. B. Y. Hsu, L. A. Perez, C. J. Takacs, G. C. Bazan and A. J.

Heeger, *Nano Lett.*, 2012, **12**, 6353–6357.

160 H. R. Tseng, H. Phan, C. Luo, M. Wang, L. A. Perez, S. N. Patel, L. Ying, E. J. Kramer, T. Q. Nguyen, G. C. Bazan and A. J. Heeger, *Adv. Mater.*, 2014, **26**, 2993–2998.

161 B. H. Lee, G. C. Bazan and A. J. Heeger, *Adv. Mater.*, 2016, **28**, 57–62.

162 S. Das, B. H. Lee, R. T. H. Linstadt, K. Cunha, Y. Li, Y. Kaufman, Z. A. Levine, B. H. Lipshutz, R. D. Lins, J.-E. Shea, A. J. Heeger and B. K. Ahn, *Nano Lett.*, 2016, **16**, 6709–6715.

163 B. H. Lee, B. B. Y. Hsu, S. N. Patel, J. Labram, C. Luo, G. C. Bazan and A. J. Heeger, *Nano Lett.*, 2016, **16**, 314–319.

164 C. Luo, A. K. K. Kyaw, L. A. Perez, S. Patel, M. Wang, B. Grimm, G. C. Bazan, E. J. Kramer and A. J. Heeger, *Nano Lett.*, 2014, **14**, 2764–2771.

165 J. Lee, S.-H. Kang, S. M. Lee, K. C. Lee, H. Yang, Y. Cho, D. Han, Y. Li, B. H. Lee and C. Yang, *Angew. Chemie Int. Ed.*, 2018, **57**, 13629–13634.

166 J. C. Wittmann and B. Lotz, *J. Polym. Sci. Polym. Phys. Ed.*, 1981, **19**, 1853–1864.

167 J. C. Wittmann, A. M. Hodge and B. Lotz, *J. Polym. Sci. Polym. Phys. Ed.*, 1983, **21**, 2495–2509.

168 J. C. Wittmann and B. Lotz, *Prog. Polym. Sci.*, 1990, **15**, 909–948.

169 C. De Rosa, C. Park, E. L. Thomas and B. Lotz, *Nature*, 2000, **405**, 433–437.

170 M. Brinkmann and J.-C. Wittmann, *Adv. Mater.*, 2006, **18**, 860–863.

171 M. Brinkmann and P. Rannou, *Adv. Funct. Mater.*, 2007, **17**, 101–108.

172 M. Brinkmann, *Macromolecules*, 2007, **40**, 7532–7541.

173 M. Brinkmann and P. Rannou, *Macromolecules*, 2009, **42**, 1125–1130.

174 A. Hamidi-Sakr, D. Schiefer, S. Covindarassou, L. Biniek, M. Sommer and M. Brinkmann, *Macromolecules*, 2016, **49**, 3452–3462.

175 C. Müller, M. Aghamohammadi, S. Himmelberger, P. Sonar, M. Garriga, A. Salleo and M. Campoy-Quiles, *Adv. Funct. Mater.*, 2013, **23**, 2368–2377.

176 E. Mohammadi, C. Zhao, Y. Meng, G. Qu, F. Zhang, X. Zhao, J. Mei, J.-M. Zuo, D. Shukla and Y. Diao, *Nat. Commun.*, 2017, **8**, 16070.

177 E. Mohammadi, C. Zhao, F. Zhang, G. Qu, S. H. Jung, Q. Zhao, C. M. Evans, J. K. Lee, D. Shukla and Y. Diao, *ACS Appl. Mater. Interfaces*, 2019, **11**, 22561–22574.

178 E. Mohammadi, G. Qu, P. Kafle, S.-H. Jung, J.-K. Lee and Y. Diao, *Mol. Syst. Des. Eng.*, , DOI:10.1039/C9ME00042A.

179 L. Biniek, B. C. Schroeder, C. B. Nielsen and I. McCulloch, *J. Mater. Chem.*, 2012, **22**, 14803.

180 D. Khim, A. Luzio, G. E. Bonacchini, G. Pace, M. J. Lee, Y.-Y. Noh and M. Caironi, *Adv. Mater.*, 2018, **1705463**, 1705463.